ADVANCED FUEL RESEARCH
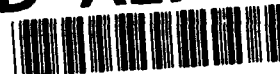
P. O. Box 380379
East Hartford, Connecticut 06138-0379
Telephone (203) 528-9806
Fax (203) 528-0648

- PHASE I -
FINAL REPORT

AD-A279 763

Advanced Fuel Research, Inc.
87 Church Street
East Hartford, Connecticut 06108

DTIC
S ELECTE
MAY 3 1 1994
F **D**

Contract Number DAAL01-93-C-4058
Project Number PF3140-8067/ACQ#3.1616

Issued
May, 1994

For the Period
July 30, 1993 to April 30,1994

"Detection of Environmental Deterioration in
Fiber Reinforced Composites by FT-Raman Spectroscopy"

Prepared by
Stuart Farquharson, Anthony Bananno, Rosemary Basilakis,
Martin Carangelo, Marie DiTaranto, John Haigis,
Kim Knight, Michael Serio and Wayne Smith

for

U.S. Department of Defense
Department of the Army
U.S. Army Research Laboratory

UNCLASSIFIED

94-15947

DTIC QUALITY INSPECTED 1

94 5 26 090

Research, analytical services and consulting for the development of new and improved clean fuels.

EXECUTIVE SUMMARY

A number of advanced fiber reinforced organic matrix composites are being developed and applied in the aerospace industry. In these applications, the composites may be exposed to a variety of harsh environments, which may induce chemical and physical changes in the composite material, and ultimately lead to component failure. The successful use of these composites, therefore, requires methods to reliably detect and assess these changes.

During this Phase I Program, a fiber optic based Fourier transform Raman spectrometer was specifically developed to perform nondestructive evaluation of environmentally damaged composites. Specifically, graphite and Kevlar reinforced epoxy and polyimide composite samples were subjected to thermal cycling, moisture exposure and ultraviolet irradiation. Three point flexure tests were used to measure flexural strength, flexural modulus, failure strain and failure load to assess induced mechanical property changes in the composites. Reflectance infrared spectra of the sample surfaces, as well as transmission infrared spectra of evolved gas phase chemical species were used to further characterize these changes.

The Raman and infrared Kevlar vibrations trend changes in flexural strength and failure strain, respectively for thermally degraded composites. These data, along with infrared spectra of evolved species, suggest thermal degradation of Kevlar/epoxy composites occurs in three stages; degradation and removal of the epoxy surface layer, followed by decomposition of the inner matrix, and degradation of Kevlar at higher temperatures. The results establish correlations between the FT-Raman and reflectance infrared spectral features *and* the mechanical property tests for the environmentally degraded composites.

This technique could be used to develop a methodology to assess in-use component health and predict component performance. Furthermore, a prototype instrument with an extended fiber optic probe could be developed with the potential of accessing an Army vehicle. This would be the subject of Phase II research.

Accesion For		
NTIS CRA&I		☑
DTIC TAB		☐
Unannounced		☐
Justification		
By		
Distribution /		
Availability Codes		
Dist	Avail and / or Special	
A-1		

"Detection of Environmental Deterioration in Fiber Reinforced Composites by FT-Raman Spectroscopy"

TABLE OF CONTENTS

1. THE PHASE I PROPOSAL

1.a. The Problem or Opportunity

A number of advanced composites are being developed and applied to Army systems. In such applications, these composites may be exposed to a variety of harsh environments, including excessive solar exposure, temperature and humidity excursions, and variations in service loadings. A combination of these effects can induce deterioration through physical, chemical, and photo-chemical mechanisms. These mechanisms are expressed in composite degradation, such as plasticization of the polymer, coating delamination, microcracking, fiber blooming, fiber/matrix debonding, and/or lowering of the glass transition temperature, all of which can lead to reduced mechanical performance and ultimately component failure. The successful use of these composites, therefore, requires methods to reliably detect and assess these changes prior to loss in mechanical properties.

1.b. The Innovation

A fiber optic based Fourier transform Raman spectrometer is proposed for the nondestructive evaluation of environmentally degraded composite materials, specifically; graphite and Kevlar reinforced epoxy and polyimide composites. The system will measure changes in chemical composition (functional groups in the base polymer, the hardener, and the coupling agent), relative percent cross-linking (allowing estimates of the glass transition temperature), and correlate this data to mechanical properties. This information will be used to assess component condition, and predict component lifetime.

The FT-Raman spectrometer will employ a flexible fiber optic cable that will allow positioning of the probe at suspect or critical components located remotely from the instrument. This will eliminate sample extraction or removal of a component from an in-use structure, which is required by most chemical and physical methods of analysis. The system will perform each analysis in approximately one minute, allowing examination of multiple sites on a structure within a relatively short time period.

1.c. The Proposal

The goal of Phase I is to analyze chemical and physical property changes of composite materials induced by temperature excursions, exposure to moisture and ultraviolet radiation, oxygen enriched environments, and various combinations. An FT-Raman spectrometer will be used to perform these measurements on graphite and Kevlar reinforced epoxy and polyimide composite samples. Spectral changes will be correlated to changes in mechanical properties, such as Young's modulus, compression modulus, and fracture toughness. Initially, a graphite/epoxy composite employing diamino diphenyl sulfone as a hardening agent will be examined to determine and design critical experiments for the other composites. The final objective of Phase I is to identify Raman spectral features that change with natural and/or accelerated weathering and can be correlated to mechanical properties, thereby demonstrating the feasibility of this technique to characterize and predict composite performance. During Phase II, a prototype instrument will be developed employing an extendable fiber optic probe for at-site inspection of components contained in or part of full-scale Army systems. In addition, laboratory research will continue to develop spectral/mechanical correlations for a wider variety of composite types, environmental damage parameters (e.g. burning), and component flaw characteristics.

2. BACKGROUND

2.a. Chemical and Physical Properties of Fiber Reinforced Composites

Recently, a number of advanced composites have been developed for their chemical, physical, electrical, and mechanical properties. Among these is a family of fiber reinforced organic matrix composites being developed for their superior engineering properties.[1] These include; formability, thermal resistance, fracture toughness, and most importantly their high strength to weight ratio. Of particular interest are graphite and Kevlar reinforced epoxy and polyimide composites, which are being extensively used in Army systems, especially aircraft components. These components can be prepared from a variety of prepreg materials, supplied by several manufactures.[2] For instance, a typical prepreg may consist of a sheet of woven carbon fibers (often pyrolyzed from polyacrylonitrile, eg. Thornel) impregnated with one or more partially cured resins (eg. diglycidyl ether of bisphenol A, DGEBA), an amine based hardener (eg. diethyl triamine), and possibly a fiber coupling agent (eg. a siloxane derivative) and/or a mold release agent (eg. a silicone coating). The prepreg is then shaped and cured in a hot press mold or autoclave according to the manufacturers temperature treatment program. During the heating, the epoxy resin chain length is extended (reaction of the epoxide ring with the phenol functionality) and the cross-linking network of the polymer is formed (reaction of the epoxide ring with the amine functionality, Figure 1). Upon cooling the molecules form an irregular three-dimensional structure held in place by dipole-dipole forces, disallowing the formation of regular crystalline lattices. It is the curing cycle that defines the extent of the network, the amount of crystalline structure, the glass transition temperature, the effectiveness of the fiber-matrix coupling agent, and ultimately determines the composite properties and useful temperature range[4,5]

Diglycidyl Ether of Bisphenol A
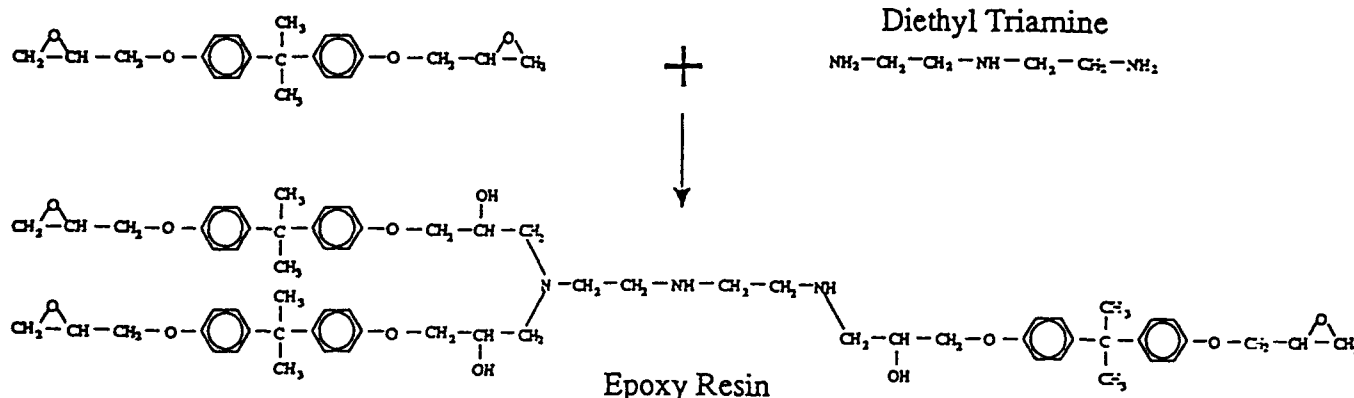
Diethyl Triamine

Epoxy Resin

Figure 1. Chemical Structures and Cure Reaction of DGEBA by Diethylene Triamine.

The successful employment of graphite/epoxy laminates as Army system components (layups, honeycomb and foam core skins, etc.) requires a method of inspection to detect and assess material property changes incurred during use. For example, a component may be exposed to an engine blast, resulting in excessive thermal changes. If sufficient, this exposure may lead to chemical decomposition, both in the polymer matrix and at the fiber-matrix interface, ultimately resulting in microcracks and delamination, respectively.[6]

A variety of methods have been employed or specifically developed to evaluate polymeric composites, and can be divided into three broad classifications: inspection techniques, mechanical property tests, and spectroscopic analysis methods. These are briefly described below.

2.b Defect Inspection Techniques

The simplest methods of evaluating a component are based on appearance. These methods have been developed to measure material flaws in composites, such as cracks, voids, delamination and deformation.[7] These methods are designed to be nondestructive and include; image analysis,[8] acoustic,[9,10] ultrasonic,[11,12] thermal emission,[13] and interferometric[14,15] measurements among others. These methods can be extremely useful in categorizing the end result of in-use damage.

2.c. Mechanical Property Tests

The selection of a polymer or composite with particular engineering characteristics has been traditional based on a number of property tests. These tests help define the useful physicochemical, mechanical, thermal, electrical, as well as environmental limits for a particular material.[6] Mechanical property tests are particularly useful in assessing the health of graphite/epoxy composites used for Army vehicle components. For example, exposure of these components to excessive temperatures can result in chemical decomposition, which is reflected in loss of mechanical strength, increased brittleness and rigidity.[6] The extent of damage can be determined by mechanical property tests, such as Young's modulus (tensile modulus), compression modulus, fracture toughness, and short beam shear. Recently, significant strides have been obtained in correlating these mechanical test values to compositional changes.[16-21]

2.d. Spectroscopic Methods of Analysis

A number of spectroscopic techniques have been used to measure chemical properties of composites. For example; NMR[22,23] has been used to measure molecular orientation and environments at nanometer scales, fluorescence[24] has been used to follow chemical changes during polymer cure and long term aging, XRD[25] has been employed to determine crystallinity at the molecular level, and DSC[26] has been used to measure the melt and glass transition temperature (which defines the useful region of thermoplastic polymers, eg. polyethylene).

Infrared spectroscopy has found wide use in measuring the cure kinetics of polymers.[16-20,28] For epoxy resins, this has been done both by imbedding fiber optics,[17,18] and by diffuse reflectance (DR) infrared spectroscopy (Figure 2).[20] These methods illustrate the ability to measure the reduction of the epoxide ring (950 cm^{-1}) and amide mode (1535 cm^{-1}) intensities and the generation of imide modes (1370 and 1710 cm^{-1}). Recently, AFR used DR infrared spectroscopy to observe thermally induced spectral changes of a cured prepreg obtained from Dow-United Technologies (Figure 3). Clear changes occur in band intensities throughout the spectrum, particularly the aromatic C-H bend (1010 cm^{-1}) and the aromatic C=C stretch (1508 cm^{-1}).

Although these techniques are very effective in measuring the chemical properties of the composites, they generally require sample extraction and preparation, restricting their use to laboratory environments. Infrared reflectance spectroscopy shows the most promise as an at-site measurement device, however, extensive optical engineering would be required to allow in-place inspection of a component.
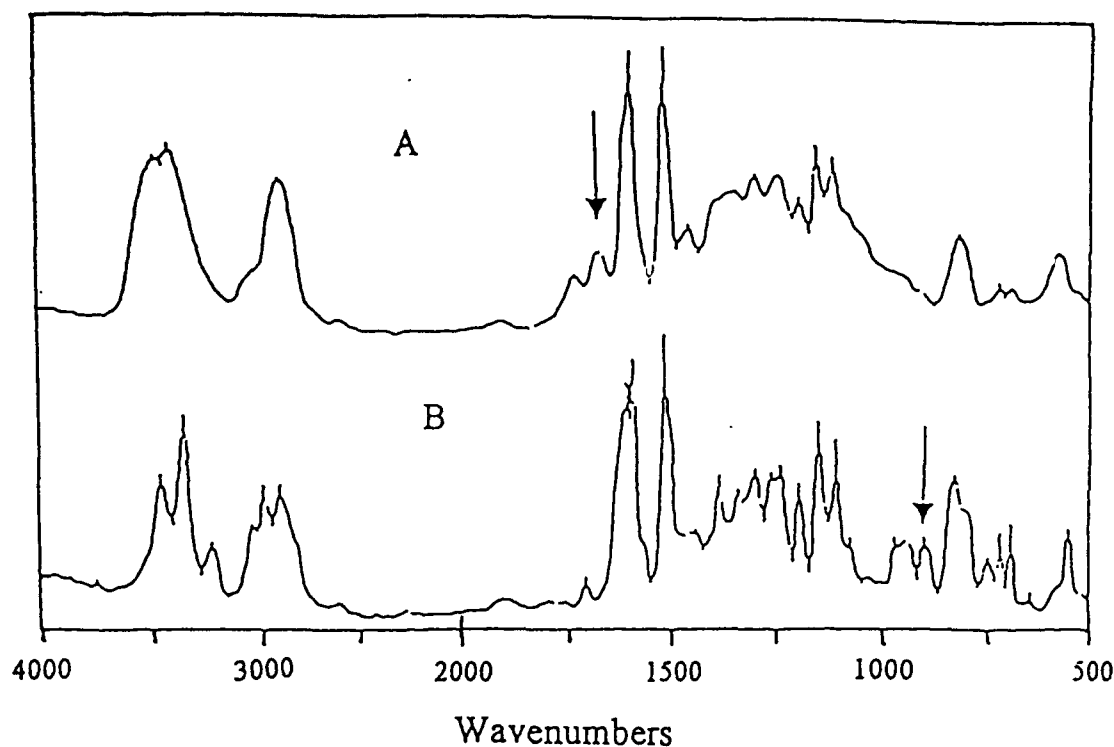
6

Figure 2. DR Infrared Spectra of Narmco Prepreg A) Before and B) After Cure. Note the Disappearance of the Epoxide Ring Modes (900-1000 cm^{-1}) and the Appearance of the Carbonyl Doublet (~1700 cm^{-1}).[20]
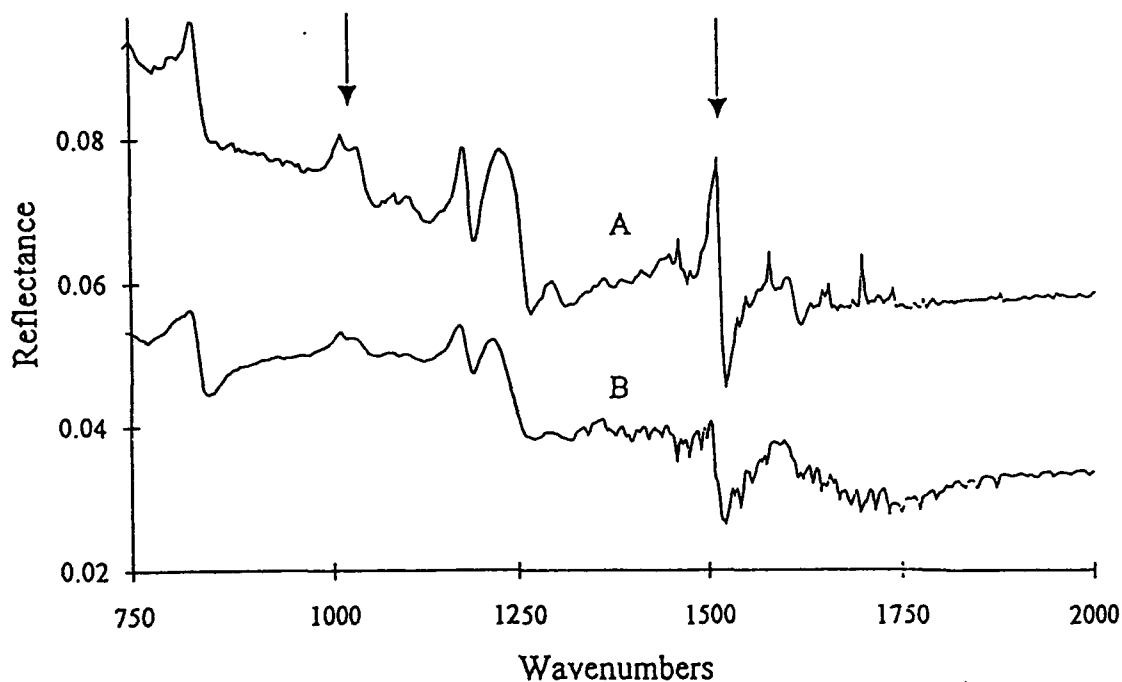

Figure 3. DR Infrared Spectra of Cured Dow-United Technologies Epoxy Composite at 25 °C A) Before and B) After Cycling to 200 °C. Note the Intensity Decrease for the Aromatic C-H Bend (1010 cm^{-1}) and the Aromatic C=C Stretch (1508 cm^{-1}).

2.e. Raman Spectroscopy

Raman spectroscopy, when coupled to sample probes *via* fiber optics, has the potential of overcoming the stringent requirements described above, and offers a unique set of advantages for *at-site* monitoring. First, Raman scattered radiation is a function of molecular vibrational frequencies and the signal intensity is linearly proportional to the chemical concentration, this allows chemical identification and quantification.[29-31] In this regard, Raman spectroscopy is complementary to infrared spectroscopy for chemical analysis. Second, the recent advances in stable interferometers used in Fourier transform spectrometers and charge coupled device detectors used in dispersive spectrometers allow measurement of complete spectral regions simultaneously.[32,33] This has eliminated the long analysis times traditionally associated with Raman, allowing near real-time and muticomponent measurements on a continuous basis. Third, Raman spectroscopy is performed typically in the visible and near infrared regions of the spectrum allowing the use of long lengths (5000 feet) of highly transmittant, inexpensive communication fiber optics.[34-40] Fourth, a fiber optic probe could be designed into a hand held device or automatic scanning system to perform nondestructive, in-place analysis without requiring sample preparation, separation, disposal or addition of reagents.[36-40]

The PI of this program has employed fiber optic Raman spectroscopy for the analysis of several polymer processes on-line. One system was designed to measure the percent crystallinity on a polyethylene blown film line,[41] while another system was employed to measure the extent-of-cure for a Dow epoxy resin (Figure 4). A ratio of the epoxide ring mode, 1250 cm^{-1} to the 1190 cm^{-1} band, or the epoxy methyne stretch, 3100 cm^{-1} to the bridging methyl stretch 2900 cm^{-1}, can be used to predict the average number of repeat units, n.
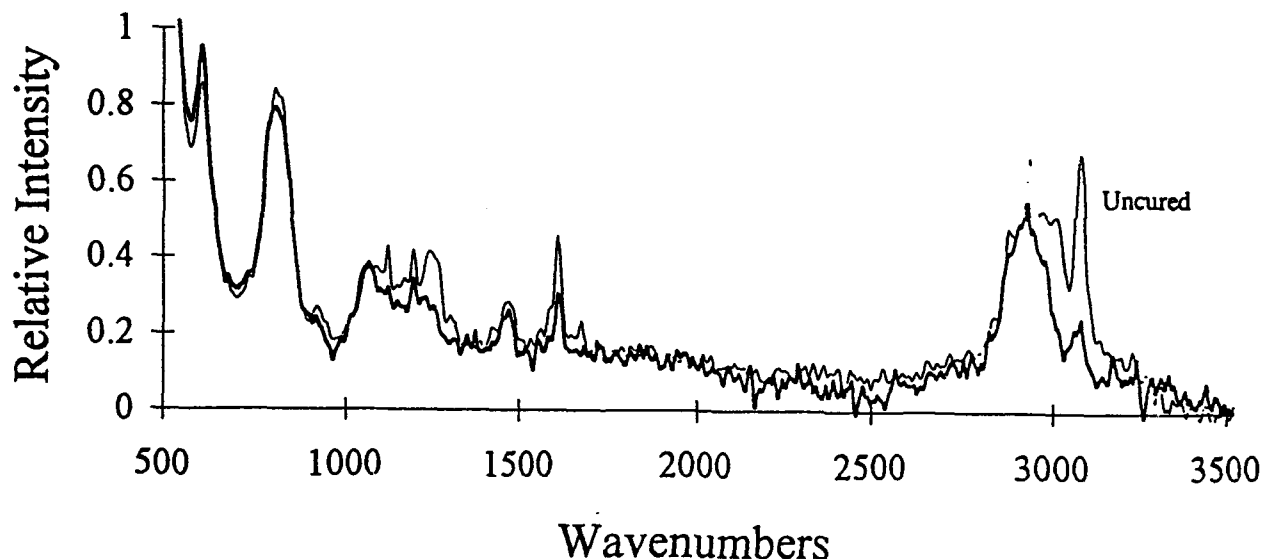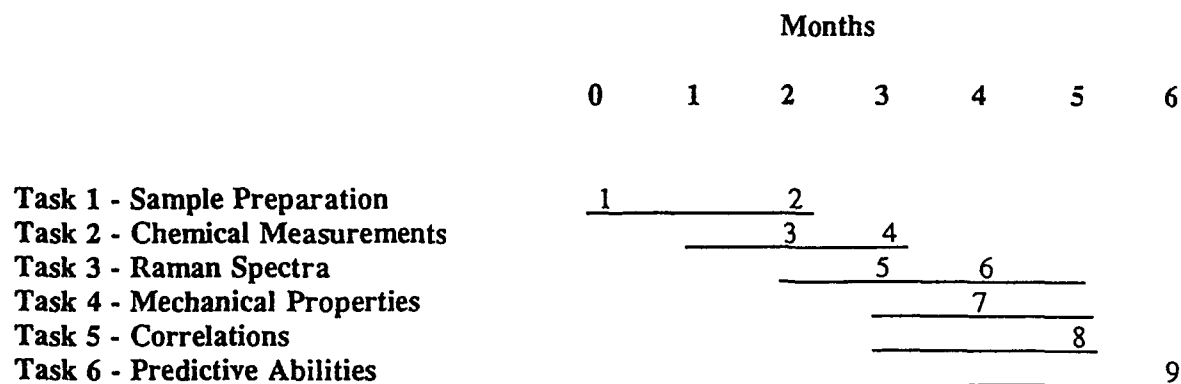

Figure 4. FT-Raman Spectra of Cured and Uncured Epoxy Resin.

2.f. The Phase I Program

Based on these advances in Raman spectroscopy, and the observation of thermally induced infrared spectral changes of a cured prepreg (*vide supra*), **AFR proposed the design of a fiber optic based Fourier transform Raman (FT-Raman) spectrometer for the nondestructive evaluation of thermal, as well as moisture and ultraviolet damaged composite materials, specifically graphite and Kevlar reinforced epoxy and polyimide laminates.** AFR proposed the following objectives to achieve this goal: 1) design and construct a fiber optic based FT-Raman spectrometer, 2) analyzing composite degradation chemistry by gas phase infrared analysis of evolved species from heated samples, and transmission infrared analysis of chemically dissolved composites, 3) prepare numerous samples by heating, ultraviolet irradiation and extensive moisture exposure, 4) measure the infrared reflectance spectra of these samples, 5) measure the Raman spectra of these samples, 6) measure the three point bend mechanical properties of these samples, 7) develop correlations, and 8) determine predictive abilities.

The final objective of Phase I is to identify Raman spectral features that changes with thermal, ultraviolet and moisture exposures, can be correlated to mechanical properties, and which in turn can be used to determine composite health and predict future performance. This would provide a bases for the development of a prototype instrument during Phase II for at-site component inspection. This Phase I program was performed according to the following schedule, and the results are summarized in the following sections of this report.

2.g. The Schedule

			Months			
0	1	2	3	4	5	6

Task 1 - Sample Preparation 1————2

Task 2 - Chemical Measurements   3——4

Task 3 - Raman Spectra   5——6——

Task 4 - Mechanical Properties   —7——

Task 5 - Correlations   ———8

Task 6 - Predictive Abilities   ———9

Milestones

1 - Sample heated   6 - DR spectra

2 - Samples exposed   7 - Lab results

3 - TG/FT-IR   8 - Chemometrics

4 - DSC, GC, fluorescence 9 - Test methodology

5 - Raman spectra

3. EXPERIMENTS AND RESULTS

3.a. The FT-Raman System

A Bomem MB-155 interferometer designed for FT-IR was modified to perform FT-Raman experiments. The primary components used to transform this instrument, were a Nd:YAG excitation laser source, an InGaAs detector, and a variety of transfer optics (see Table 1 and Figure 5). Furthermore, fiber optic sample probes were designed and built to perform measurements remote from the spectrometer. The Nd:YAG laser generated Stokes Raman scattering in the near infrared region from 1.064 to 1.852 µm corresponding to 9398 to 5398 absolute cm^{-1} or 0 to 4000 shifted cm^{-1} (Δcm^{-1}, Figure 6). Consequently, the InGaAs detector and fiber optics were chosen for optimum performance between 1 and 2 µm. The instrument has undergone continuous improvement throughout the Phase I program. The current design can be described in terms of its optical, electronic, and data reduction systems.

3.a.1. Optical System

The output of the Nd:YAG laser (up to 5W) passes first through a holographic bandpass filter, which removes plasma lines generated by the laser krypton flash lamps (50% transmission at 90°, Figure 7), through a focusing lens (f/2) and into the source optical fiber (numerical aperture of 0.22). The plasma filter is mounted on a pitch and yaw platform, while the lens and fiber are mounted in an XYZ translation stage also equipped for pitch and yaw. Both the platform and stage are mounted on an optical base directly attached to the laser head, thereby maintaining optical alignment throughout experiments. A power meter was used to optimize alignment and measure laser power at the sample for each experiment. Typically, greater than 80% of the laser power was coupled into the source fiber and transmitted to the sample.

Numerous fiber optic probes (all 3 meters in length) were constructed to optimize collection of Raman scattered radiation (see below). The source fiber, probe and collection fibers were terminated in SMA or ST fittings to allow ease of coupling. All fibers were smoothed with a series of polishing papers to 0.5 µm and examined under magnification prior to use. Samples were placed on a micrometer driven stage allowing precise control of the probe to sample distance. A rotational stage, consisting of a plexiglass plate mounted to a 2 inch fan (Sprite, ComAir/Rotron) was used for heat sensitive samples.

The collection fibers were mounted in an XYZ translation stage and placed within the focal point of an f/2 collimating lens. Two holographic Notch filters were placed in series at the interferometer side (emission) port to pass Raman, but reject Raleigh scattered light. The collimated signal is divided by a KCl beam splitter between the two interferometer optical "arms", is recombined and exits at the interferometer top (transmission) port. The beam is then collected and focused by an off-axis parabolic mirror onto the InGaAs detector element. The detector position was optimized with an XYZ stage. A cutoff filter was placed in front of the detector to reject stray laser emissions from the internal HeNe clocking laser. Furthermore, an interference filter was placed in the optical path of this clocking laser to eliminate its plasma lines from entering the detector.

The optical components of this system were selected to achieve maximum throughput. This involves both passive and active optics. The former include the plasma line filter, the holographic notch filters, the interferometer's entrance and exit windows, beam splitter and corner cube reflectors, and the HeNe rejection filter. The latter includes the laser focusing optics, each end of the fiber optic probe, the
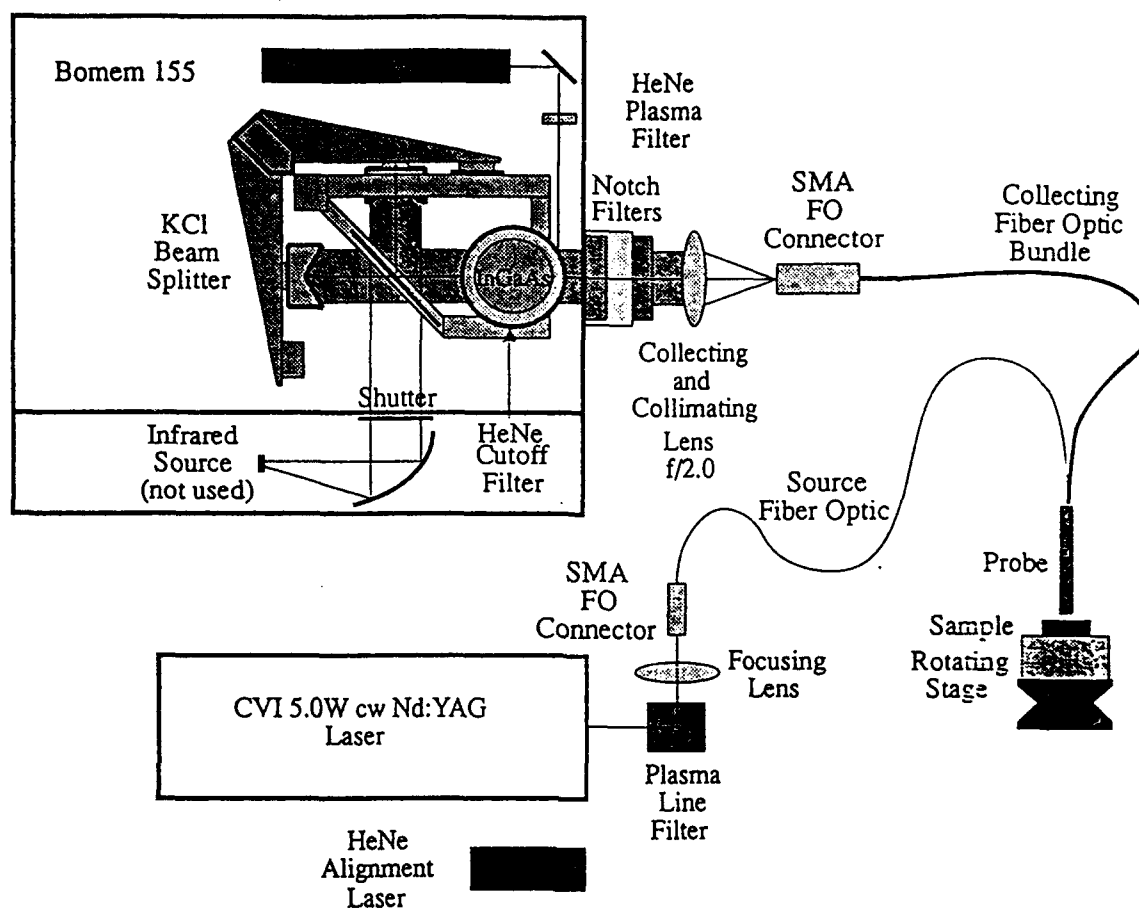
10

Figure 5. Schematic of Fiber Optic FT-Raman Design.

Table 1. FT-Raman System Components.

Component	Supplier
Bomem interferometer, model 155	Bomem, Quebec, Canada
Nd:YAG laser, model C-105	CVI Lasers, Albuquerque, NM
InGaAs detector,	Electro-Optical Systems, Inc., Pheonixville, PA
microbench optics rail	Spindler & Hoyer, Milford, MA
plasma line filter, HLBF-1064	Kaiser Optical Systems, Ann Arbor, MI
f/2 focusing lens, model 31855	Edmund Scientific
200 um fiber optic, model Anhydroguide	Fiber Guide Ind., Stirling, NJ
SMA 905 connecter	OFTI, Westford, MA
tilt stage, model 33499	Edmund Scientific
fiber optic probe	In-house design
600 um fiber optics, model	AnhydroguideFiber Guide Ind., Stirling, NJ
XYZ translation stage, model MT-XYZ	Newport, Irvine CA
f/0.75 collimating lens, model KBX043.33	Newport
Notch filter, model HNDF-1064-1.0	Kaiser Optical Systems, Ann Arbor, MI
cutoff filter, model RG850	Edmund Scientific

11

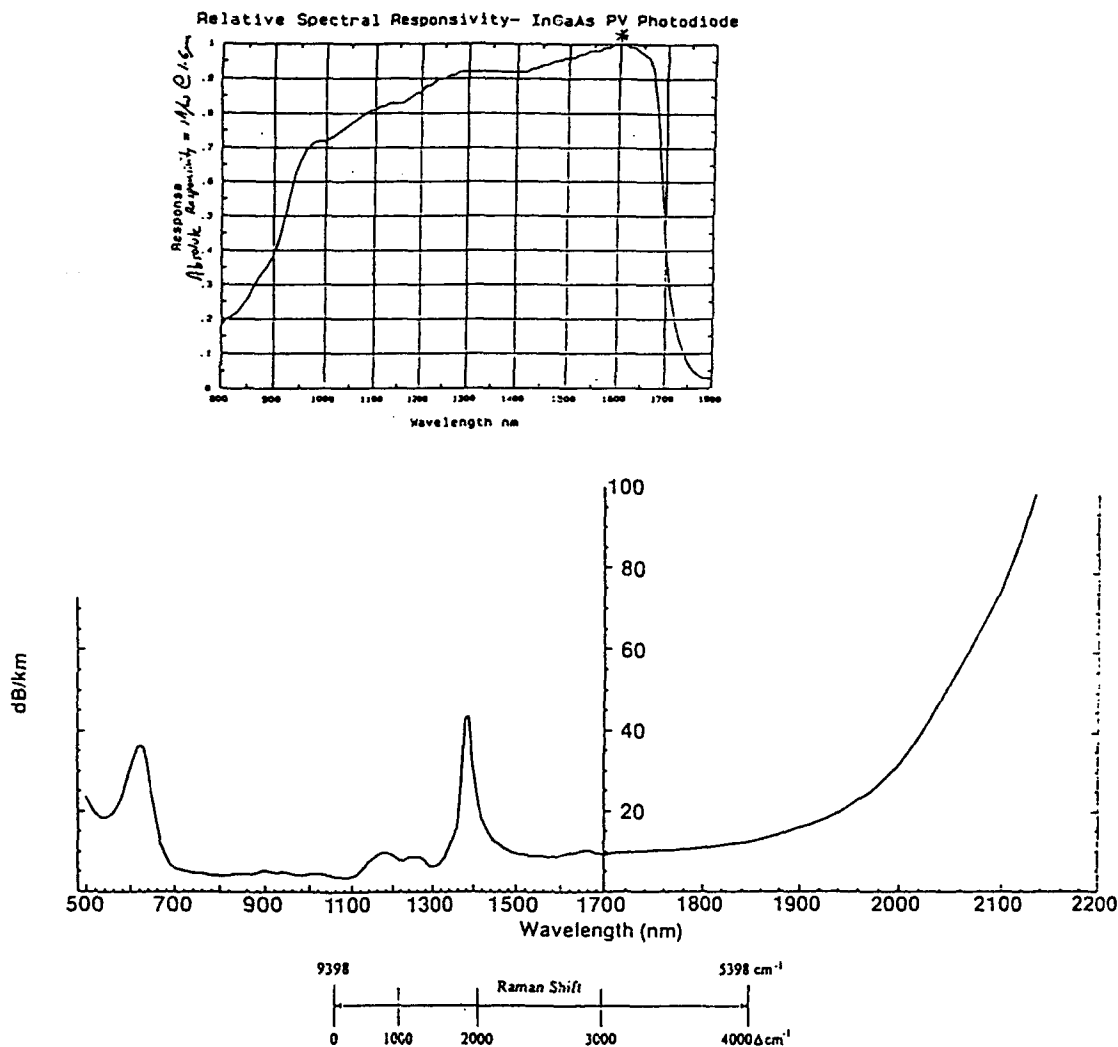Relative Spectral Responsivity- InGaAs PV Photodiode

Figure 6. A) Spectral Response Curve for InGaAs Supplied by Electro-Optical Systems (OES), B) Spectral Attenuation for Ensign Bickford Low OH⁻ Hard Clad Silica Fiber Optics.

collection and collimating optics, the detector off-axis parabolic focusing mirror, and depending upon design, the probe optics. The passive optics have little or no effect on the optical beam shape, but lower throughput due to reflection or absorption. The active optics, however, require matching each component's optical throughput (invariance) to maximize efficiency.[42] For example, the f/# of the collecting lens must be selected to match the numerical aperture of the signal fiber.
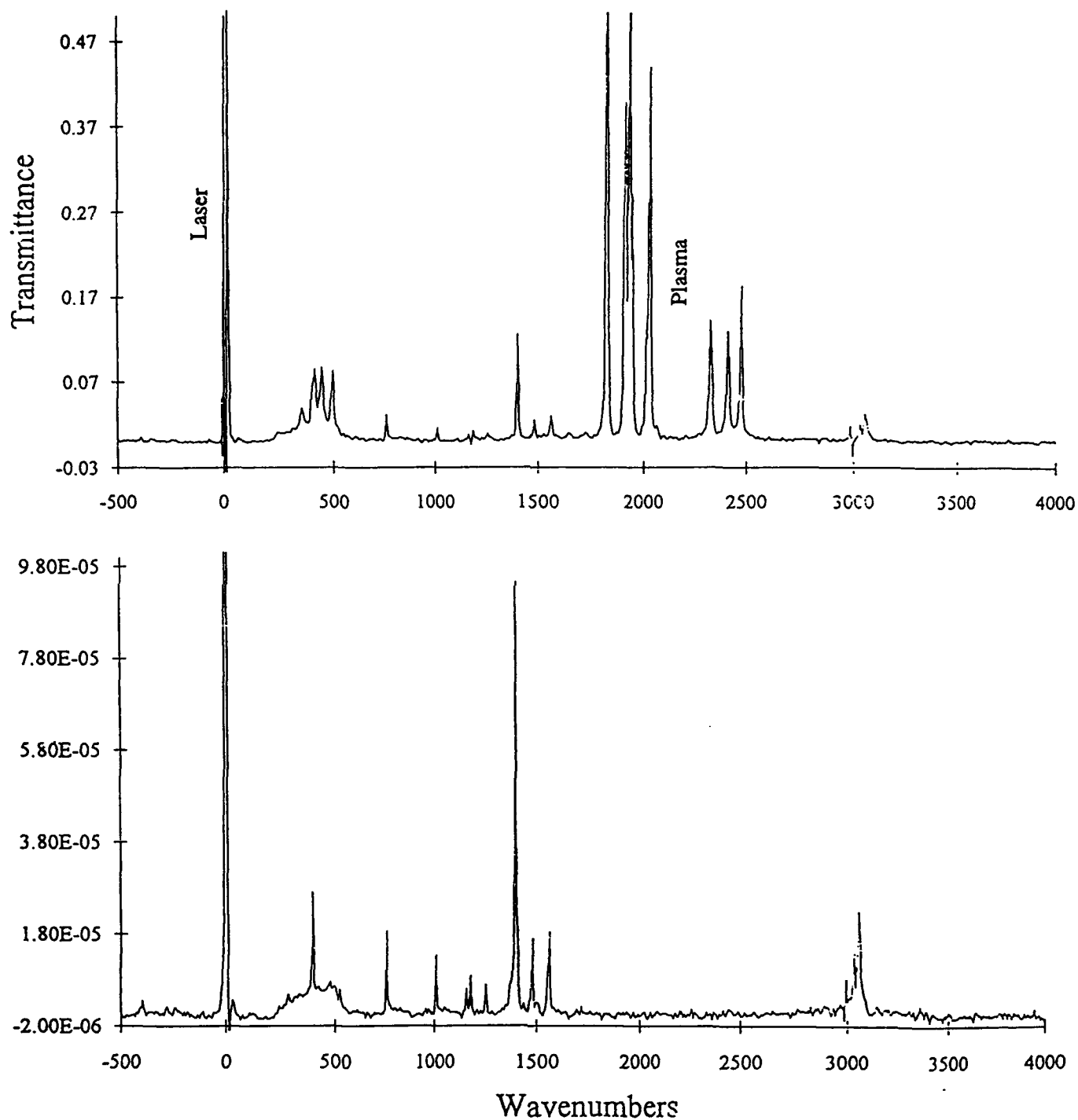
12

Figure 7. FT-Raman Spectrum of Anthracene, A) Dominated by Laser Plasma Lines, B) with Plasma Lines Removed.

Furthermore, it must be designed to properly match the spectrometer and the detector, while taking dispersion into account. Optimum coupling to the detector is of special interest, since its capacitance is directly related to its area, which determines the amount of electronic gain possible in the preamplifier. Several commercial instruments employ rather large area InGaAs detectors (3 mm diameter) and consequently have minimum gain. Therefore, the detector should be as small as possible, yet no smaller than the size of the sample imaged on the detector. The image is dictated by the fiber optics and the detector fore optics, i.e. the optical throughput should match for these two elements. The optical throughput (OT) is defined as the product of the image area and its solid angle, *viz*:

$$\text{Optical Throughput} = [\pi r^2][2\pi(1-\cos\theta)]$$

The initial fiber optic probe consisted of four 600 µm with a 200 µm gap (source fiber) yielding an image radius of 700 µm. The numerical aperture of the fibers is 0.22 corresponding to a dispersive angle of 25.4° (NA = sin θ/2) or 0.444 radians, and an OT of 0.24 mm² steradians. The Bomem detector had a 0.25 mm radius with a 1" f/1 collecting/focusing parabolic mirror corresponding to a focusing angle of 26.6° (radius/focal length = tan θ/2) or 0.92 radians, and an OT of 0.13 mm² steradians. This represents 45% detector overfill or lost light energy. For this reason, we selected the next size detector having a 0.5 mm radius and an OT of 0.52 mm² steradians allowing 100% light collection. Yet the detector is underfilled with a coupling efficiency of only 46%. This also results in a reduction of the capacitance limited gain. To offset this loss, an 18 around 1 fiber optic probe was built. All fibers were 365 µm yielding an effective radius of 912 µm and an OT of 0.41 mm² steradians and a coupling efficiency of 79%. The effect of this collection efficiency is shown in Figure 8.

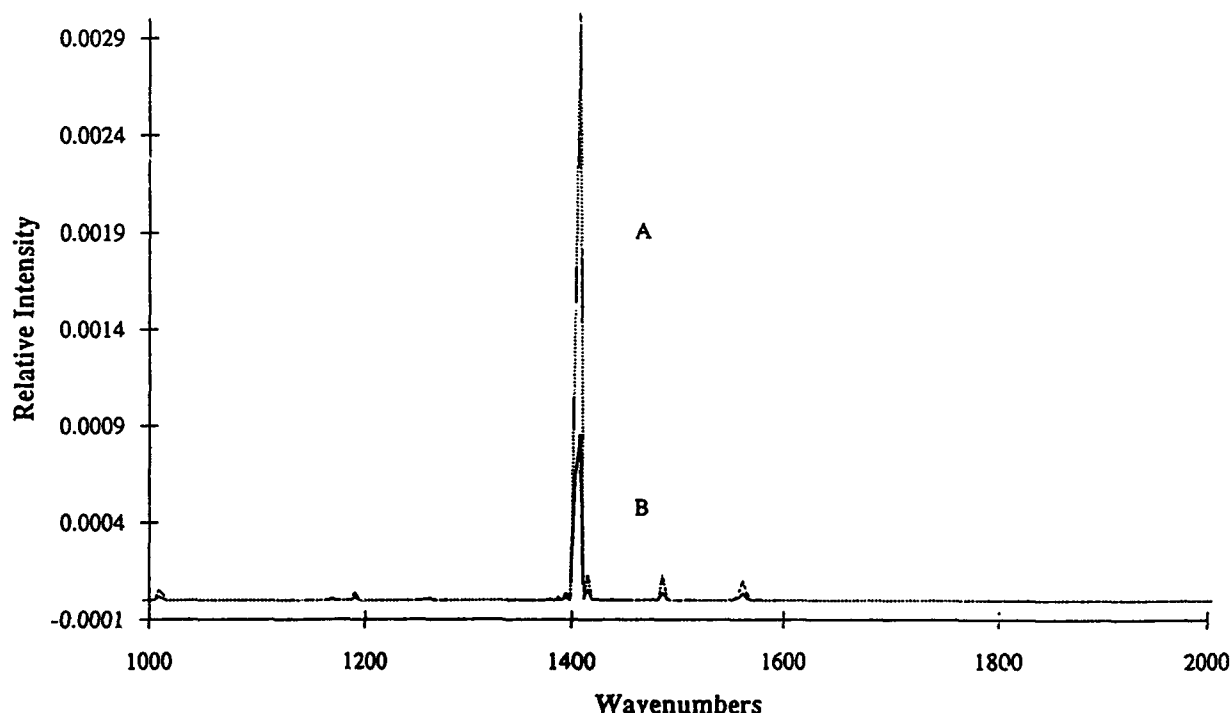Figure 8. Signal Intensity for Anthracene Ring Breathing Mode (1400 Δcm⁻¹) for A) 1 by 18 and B) 1 by 4 Fiber Optic Probes.

3.a.2. Electronic System

As previously reported, the original InGaAs detector was replaced by one with a specified diameter size and pre-amp feedback resistor to maximize optical sensitivity and electronic amplification. A schematic of the detector and supporting electronic amplifier stages are shown in Figure 9.
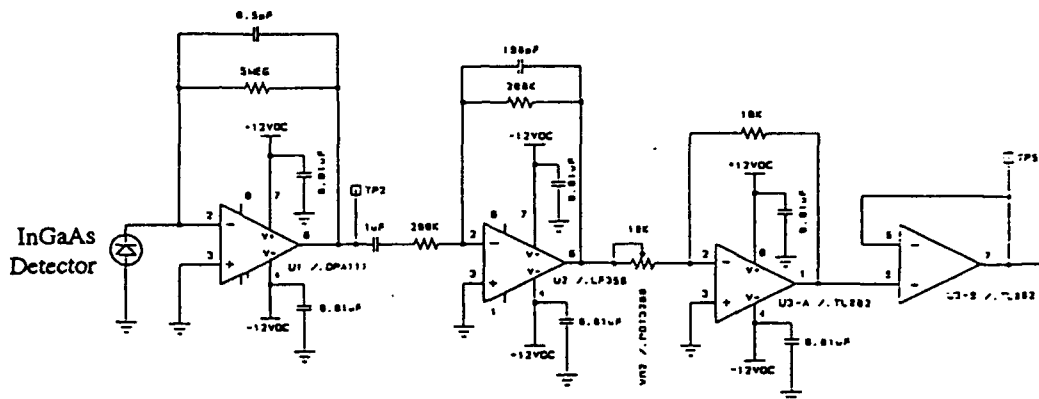

Figure 9. Schematic of InGaAs Detector, Pre-Amp, Frequency Band Pass Filter Op-Amp, Variable Gain Op-Amp, and Non-Inverting Unity Gain Op-Amp Follower.

The InGaAs detector is configured as a transresistance amplifier with a 50 MΩ feedback resistor and a 0.636 pF stray capacitor (parasitic). This pre-amplifier stage is contained in the detector assembly eliminating the RF noise observed in the original Bomem detector. The chosen resistor/capacitor combination yields a high frequency 3dB roll-off of 5 kHz ($1/(2\pi RC)$). With a 0.4 cm/s optical scan speed (0.1 cm/s physical scan speed, but x4 for Bomem since both mirrors move) this allows an optical bandwidth out to 12,500 cm^{-1} (defining an anti-Stokes Raman limit of -3100 Δcm^{-1}).

The electrical output of the detector/pre-amp combination feeds into three more op-amp stages. The first of these stages is a band pass filter with unity gain (matching input and feedback resistors, 200 kΩ). The input capacitor (1 μf, corresponding to 0.79 Hz and 2 cm^{-1}) and a feedback capacitor (190 pf, corresponding to 4182 Hz and 10456 cm^{-1}) filter high and low frequencies, providing a detection range between 9396 and -1058 Δcm^{-1}. This, along with the wavelength response optimized between 6000 and 10500 cm^{-1} (1.66 and 0.95 μm, Figure 6a), adequately covers the required 0 to 4000 Δcm^{-1}. The Bomem detector was designed with a frequency band pass between 0.3 Hz and 3.5 kHz corresponding to 9398 and 648 Δcm^{-1}, i.e. 25% loss at 648 Δcm^{-1}!

The second op-amp employs a 10K feedback resister and variable 10K input resister allowing variable gain from 1 to infinity. The last stage is a non-inverting unity gain follower. All three op-amp stages are housed in an RF shielded enclosure.

3.a.3. Data Reduction

The Bomem system allows two data reduction methods. One employs direct signal processing (DSP) electronics, the other employs digital memory access (DMA) acquisition electronics. The DMA requires collecting and averaging scans prior to the transformation, and only allows observation of interferograms in real time. The DSP performs a fast Fourier transform on each forward and backward scan generated interferogram, allowing observation of spectra in real time, and is preferred.

Previously, we described the observation of significant noise associated with one scan direction (defined as the backward scan for convenience, Figure 10). The source of this noise was identified as a miss selection of the interferogram center burst in the backward direction (and consequently the zero retardation point used in the Fourier transform equation). The DSP data acquisition electronics initially searches for a maximum to define the center burst of the interferogram. This search begins at opposite ends of the interferogram for each scan direction. Furthermore, a phase correction is generated based on the initial forward scan and then applied to all subsequent scans. For weak signals (as in the case of Raman), the interferogram maximum may be indiscernible resulting in a displacement of the center burst and application of a frequency shifted phase correction. This missapplication of the phase correction can result in significant noise throughout the spectrum, even negative values.[42] Indeed, significant improvement was obtained by collecting separate forward and backward interferograms (resulting in a well defined center burst), transforming them to spectra, THEN co-adding them. This was accomplished using the DMA acquisition electronics. As previously stated, these electronics do not allow visual inspection of the spectrum in real-time, which makes sample/optical alignment both time consuming and cumbersome.

To eliminate these problems, we have designed our own collect program using LabVIEW (National Instruments), which employs an electronics interface (general purpose instrumentation bus, GPIB) designed and constructed by On-Line Technologies, Inc. (an AFR affiliate). This program allows simultaneous observation of the interferogram and spectrum allowing quick and easy sample alignment. Initially, we designed a program to preselect (force center) the position of the center burst, for each scan direction. This eliminating directional scan-to-scan frequency shifts. However, it was found that changing sample optical geometries required redefining the center burst. To circumvent this limitation, we calculated the magnitude spectrum from the interferogram. This method takes the square root of the sum of the squares of the real and imaginary parts of the Fourier transform, eliminating the need for a phase correction. This method is generally not used (not required in
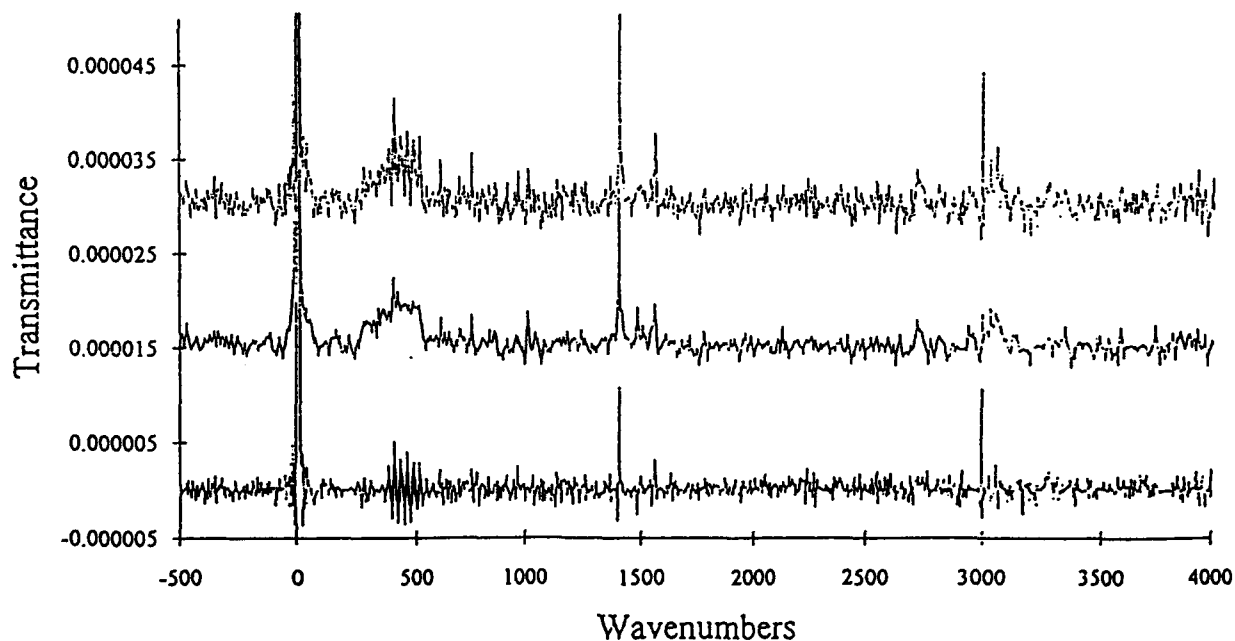

Figure 10. FT-Raman Spectrum of Anthracene, A) Forward and Backward Mirror Scans Separated into B) Forward and C) Backward.

16

infrared measurements, where the center burst is always discernable) since the noise at any wavelength is always positive and approximately doubled. This noise is insignificant compared to the noise generated by an imperfect phase correction. The LabVIEW "wire" diagram is shown in Figure 11. As shown, the program is set to collect 200 scans, compute and display both interferograms and spectra for each scan (Figure 12). The spectra are converted to Raman shift wavenumbers, by defining 9398 cm^{-1} (the Nd:YAG laser wavelength) as $0 \ \Delta$ cm^{-1}, displaying -100 to 4000 Δ cm^{-1}, and storing spectra into Excel (Microsoft) and/or Grams (Galactic) files.
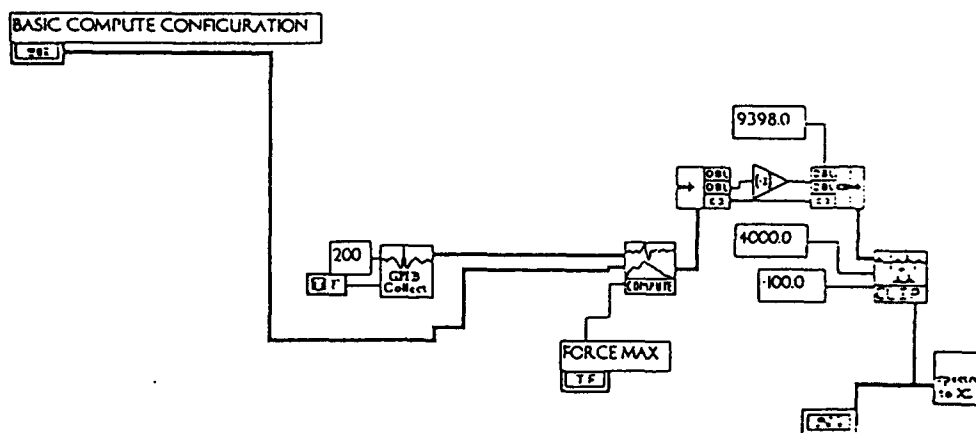
Figure 11. LabVIEW "Wire" Diagram Illustrating Data Collection and Display Components.
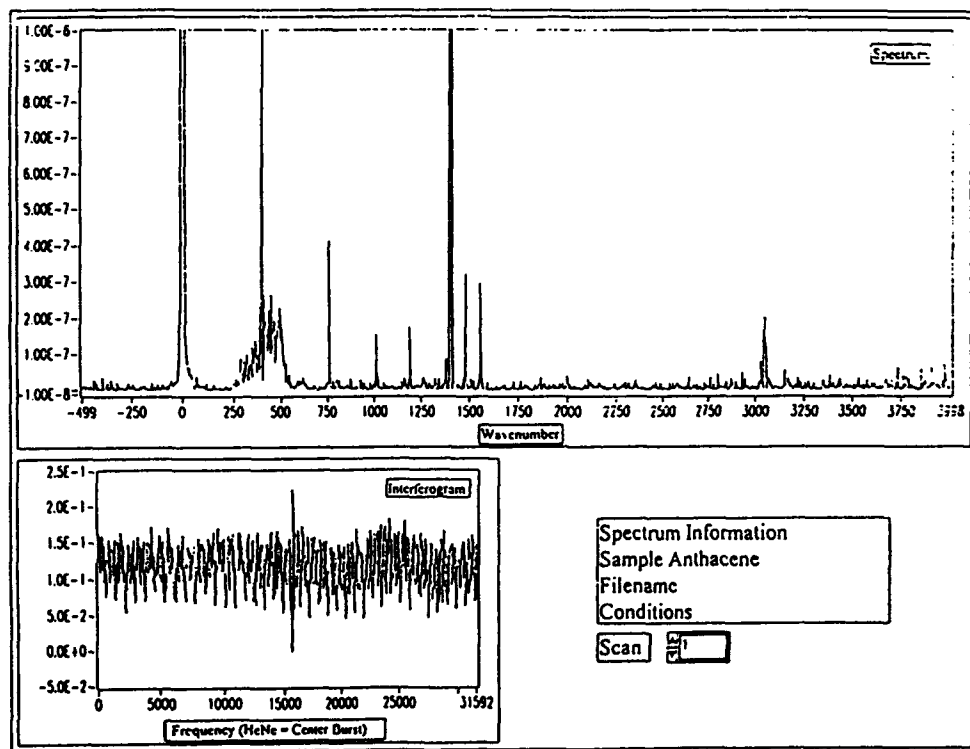

Figure 12. LabVIEW Screen Display for Raman Spectral Alignment and Collection Programs.

The improvements are demonstrated in Figure 13. The top spectrum represents 0.60W of laser power, the Bomem InGaAs detector, the 1x4 probe, 200 averaged scans, 8 cm^{-1} resolution, and a signal to noise ratio of 140 (signal equals average of three center points of anthracene 1400 cm^{-1} peak, noise equals standard deviation of baseline calculated from 1750 to 2750 cm^{-1}). The bottom spectrum represents, 0.25W of laser power, the OES InGaAs detector, the 1x18 probe, 20 averaged scans transformed as a magnitude spectrum, 8 cm^{-1} resolution and a S/N of 33,500. This, taking into account collection times and laser power, is an improvement in S/N of 575 times! These improvements allowed rapid analysis of samples. For example, powdered samples could be measured by placing the probe 1mm from the sample, and solvents by simply holding the probe against the outer glass wall of the solvent bottle Figure 14).
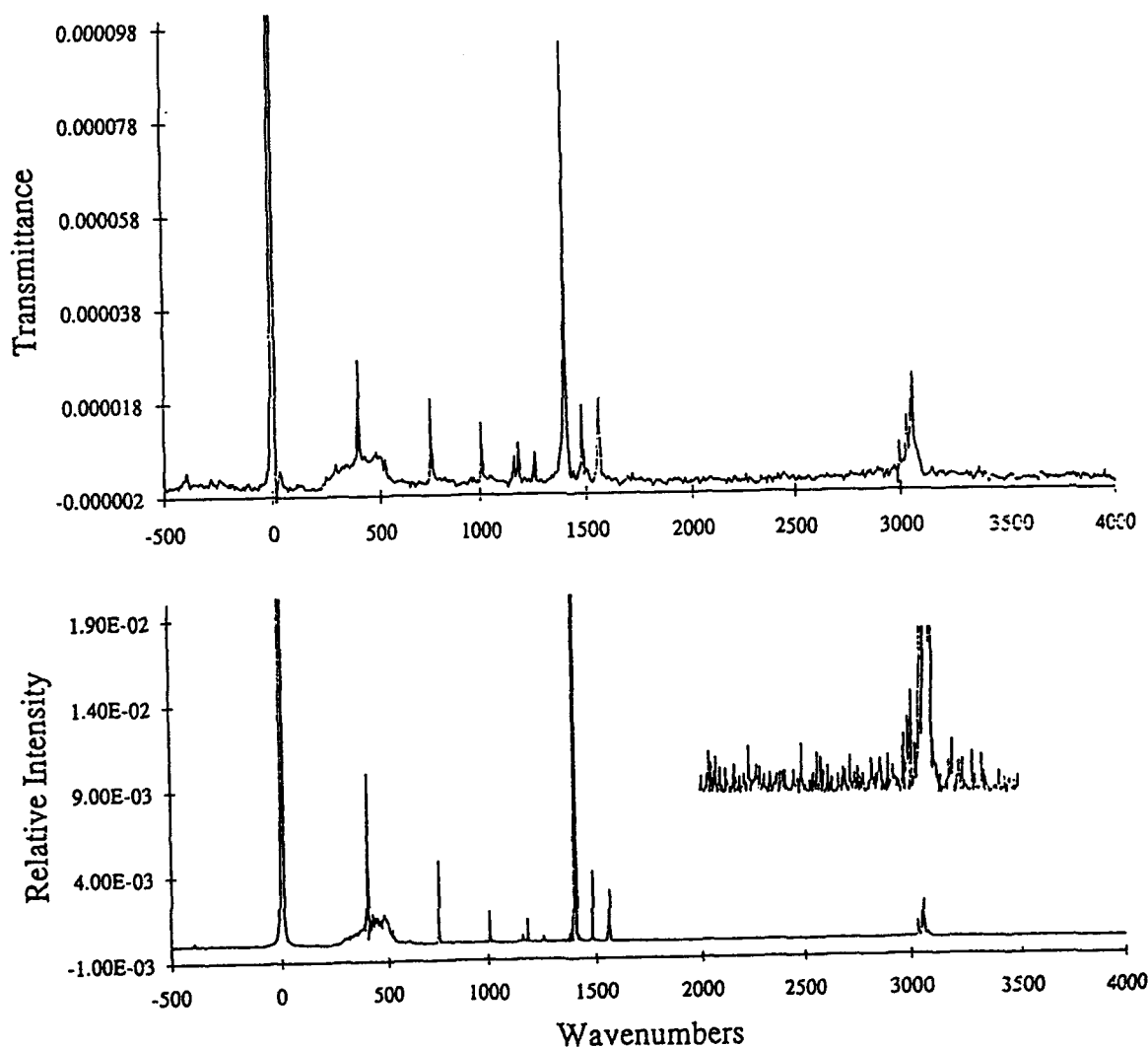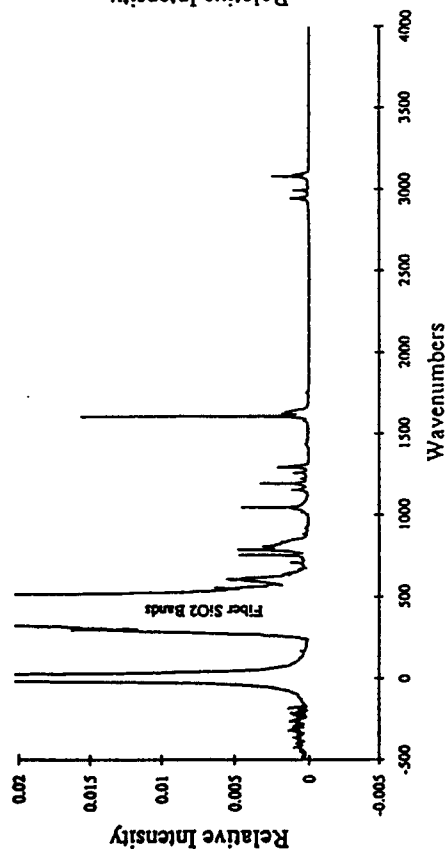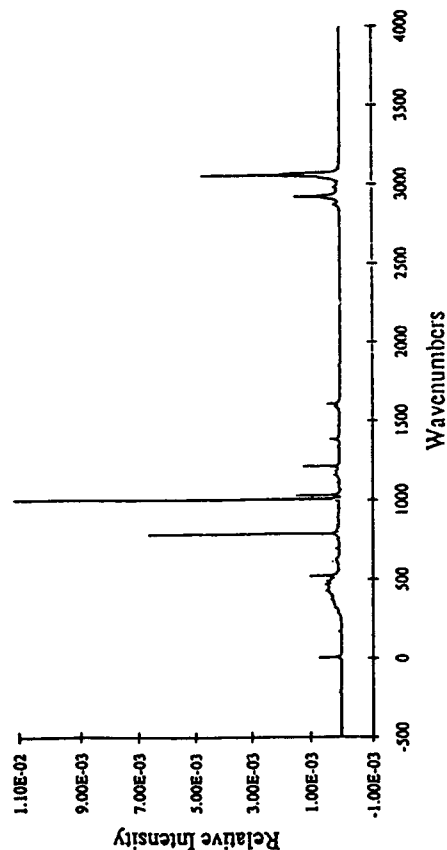
Figure 13. FT-Raman Spectra of Anthracene, A) Bomem Detector, B) OES Detector, Force Center, C) OES Detector, Magnitude Spectrum. Note Baseline Spectral Noise in Inset.
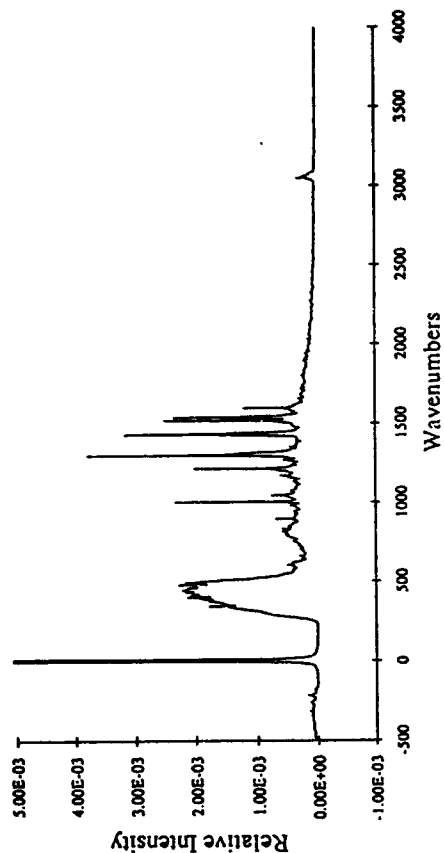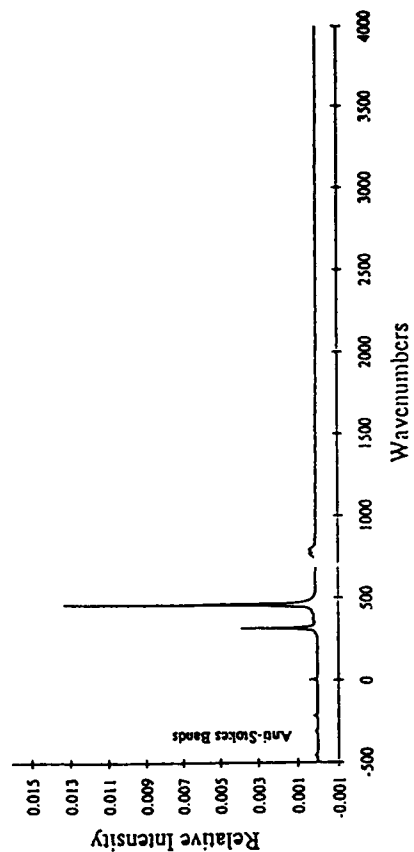
18

Figure 14. Spectra of Aspirin, Rubrene, Toluene, and Carbon Tetrachloride. All Magnitude Spectra.

3.b. Task 1 - Sample Preparation

3.b.1. Samples from United Technologies / Pratt & Whitney (UT-PW)

Three composite sheets were obtained from United Technologies / Pratt & Whitney (East Hartford, CT) courtesy of Dr. Charles Watson. One sheet consists of Hexcel F263 epoxy resin imbedded with four plies of AS4-8H5 (8 Harness Satin weave) carbon fabric and one ply of electrical grade fiberglass (E glass style 120, mounting side) cured at 350 °C for 2 hours yielding an overall thickness of 1.5 mm. The second sheet consists of Hexcel F161 epoxy resin imbedded with six plies of Kevlar (5 Harness Satin weave) and one ply of E glass in Hexcel F263 on each side. Although, this sheet was intended to be a polyimide (imbedded with Kevlar), TG/FTIR analysis of this sample revealed it to also be a graphite reinforced epoxy resin. A polyimide composite embedded with graphite fibers was, however, obtained from Case Western Reserve University (PMR-15, courtesy of Dr. Fred Lizy).

The three composites are defined as follows:

Composite #1 = Graphite Reinforced Epoxy Resin (Hexcel F263)
Composite #2 = Kevlar Reinforced Epoxy Resin (Hexcel F161)
Composite #3 = Graphite Reinforced Polyimide (PMR-15)

The following procedure was designed to generate the samples appropriate to this research program.

Step 1 Cut Samples (according to ASTM D-790-86)
        Remove E-glass from Composite #1 and #2, cut all composites to 1" x 3"

Step 2 Heat Samples for 10 minutes (2 samples each, in 2" furnace, use vent!)
        Composite #1 - 100, 125, 150, 175, 200, 220, 240, 260, 280, 300, 320, 340, 360 °C
        Composite #2 - 100, 125, 150, 175, 200, 225, 250, 275, 300, 320, 340, 360, 380, 400 °C
        Composite #3 - 100, 200, 300, 400, 500 °C (limited sample supply)

Step 3 Soak Samples in Water
        Composites #1 and #2 - native in 25 °C water for 10, 30 and 100 hours
        Composites #1 and #2 - native in 100 °C water for 1, 3 and 10 hours
        Composite #3 boiling water only

Step 4 UV Exposure (Oriel Solar simulator)
        Composites #1 and #2 - UV expose native for 1, 3, 10, 30, 100 hours in air, and in an
        enriched oxygen atmosphere (40% oxygen)
        Composite #3 10 and 100 hours only.

Step 5 Obtain Spectra
        All Composite samples - Diffuse Reflectance, Kubelka-Munk Units
        All Composite samples - FT-Raman, spin to minimize thermal heating

Step 6 Mechanical Tests
        Selected Samples - Three Point Bending - Failure Load, Failure Strain, Flexural Strength and
        Flexural Modulus

3.b.2. Thermal Degradation

Previously, a tube furnace was designed and constructed to perform thermal cycling experiments. This system was successful in preparing the graphite/epoxy composites, and will be used for the materials of this program. This furnace design (Figure 4) consists of an 8" long 2" internal diameter Mullite ceramic tube, wrapped by Kanthal resistance wire connected to a Variac (Staco Energy Products, Dayton, OH, Figure 12). The tube was further wrapped in 1" thick ceramic cloth, a portion of which served as a cover during experiments. Tin foil was used to position the composite plaques vertically in the center of the tube. The tip of a type-K thermocouple, connected to a microprocessor thermometer (Omega, Stamford, CT), was placed in close proximity of the composite plaques to measure and control the furnace air temperature. (Contact with the sample and cell walls was avoided.) The Variac on/off switch was used to control temperature to ±5 °C. Previous work showed that the experimental error in exposure times (primarily due to sample handling) is approximately ±0.5 minutes. Since this would yield large relative errors for short exposures (eg. up to 50% for 2 minute exposures), samples were exposed for periods of 10 minutes allowing greater precision in controlling exposure periods. The temperature was recorded every minute, resulting in ten values which were averaged and recorded as the actual exposure temperature. A vent was placed directly over the furnace to collect all fumes generated by thermal decomposition.
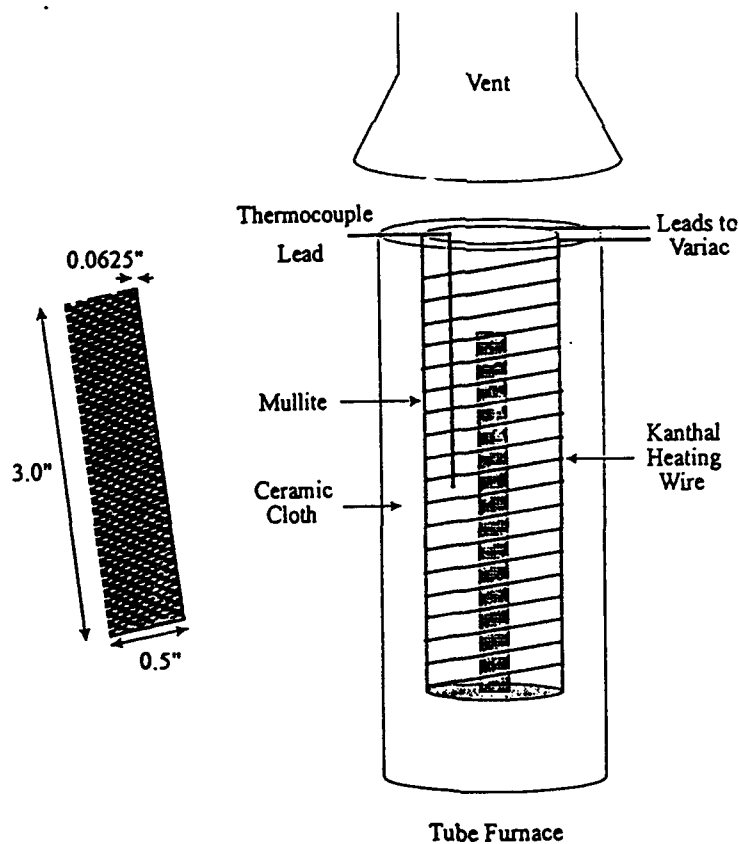

Figure 15. Dimensions and Orientation of a Carbon/Epoxy Composite Sample Plaque and Tube Furnace.

3.b.3. Ultraviolet Exposure

An Oriel 150 watt xenon arc lamp (Solar Simulator) was purchased and used in these experiments. A gas enclosed chamber with ultraviolet transparent windows was designed and constructed to perform these experiments (Figure 16). The cell is composed of a plexiglass cylinder, which has an f/1 lens to expand the beam to a four inch diameter circle allowing exposure of two plaques per run. The back wall is removable to allow easy sample replacement. Swagelock fittings have been attached to the wall of the cylinder to allow controlling the atmosphere (oxygen or nitrogen) during exposures. For safety reasons, the UV Solar Simulator was placed within the confines of three temporary walls to eliminate possible eye exposure, the exit port of the plexiglass "controlled atmosphere" cell was tied into a vent, and 40% oxygen was used in the enriched experiments to eliminate possible fire or over exposure hazards. Finally, an electric timer was employed to automatically shut off the Simulator lamp, as well as the gas flows into the chamber at the end of each exposure period.
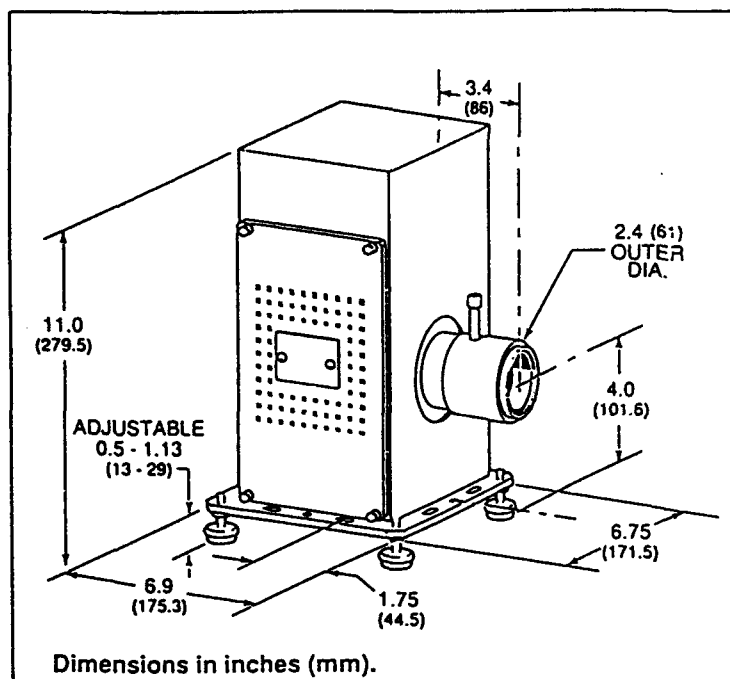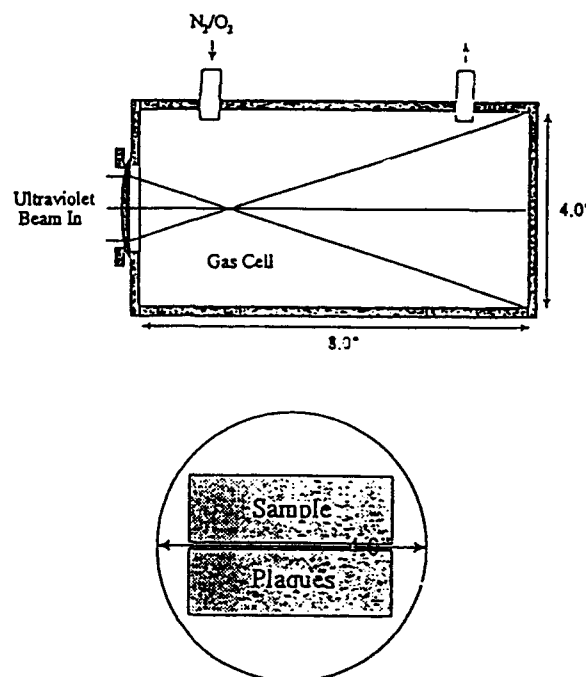

Dimensions of the 86000 Solar Simulator.

Figure 16. A Side View of the Solar Simulator and the Gas Cell for Photo-Oxidative Exposure.

3.b.4. Moisture Exposure

We initially proposed using an environmental chamber (60 °C, 95% humidity at UT-PW) to mimic moisture exposure. However, discussions with Dr. Watson suggested that the effects of water on composite materials could be simulated in accelerated tests by simple exposure to boiling water. In principle, there are two possible effects which can result from exposure to moisture. The water can be absorbed within the molecular framework of the composite reversibly or irreversibly. In the former case, no chemical changes occur and little or no physical property changes are expected. (It is realized that absorption along the fiber interface can change the composite properties.) It is the latter case which is of interest here, in which changes in chemical structure will be investigated by Raman spectroscopy. For this reason, the samples will be exposed according to the schedule listed above in an attempt to generate irreversible chemical changes.

3.c. Task 2 - Chemical Measurements

3.c.1. Sample characterization by thermogravimetric / FT-IR analysis (TG/plus).

In an effort to understand the decomposition chemistry due to the three different environmental exposures, several methods were chosen to initiate decomposition. One method employs sample pyrolysis to generate evolved gas phase chemical components and chemical products from the composite material. The second method involves exposure to chemical solvents, oxidants and acid halides.

3.c.2. Composite #1 = Graphite Reinforced Epoxy Resin (Hexcel F263)

A TG/plus instrument (patented by AFR and licensed to Bomem) was used to pyrolyze a small sample of each composite. The TG/plus instrument consisted of a DuPont 951 TGA, a Bomem model 100 FT-IR equipped with an MCT detector, and an Infrared Analysis, Inc.16 pass gas cell with coupling optics. A helium sweep gas (250 cm³/min) is employed to bring evolved products from the TGA into the gas cell. A 10 milligram sample was cut from the center portion of Composite #1 and heated according to the temperature pyrolysis and combustion program profile shown in Figure 17.
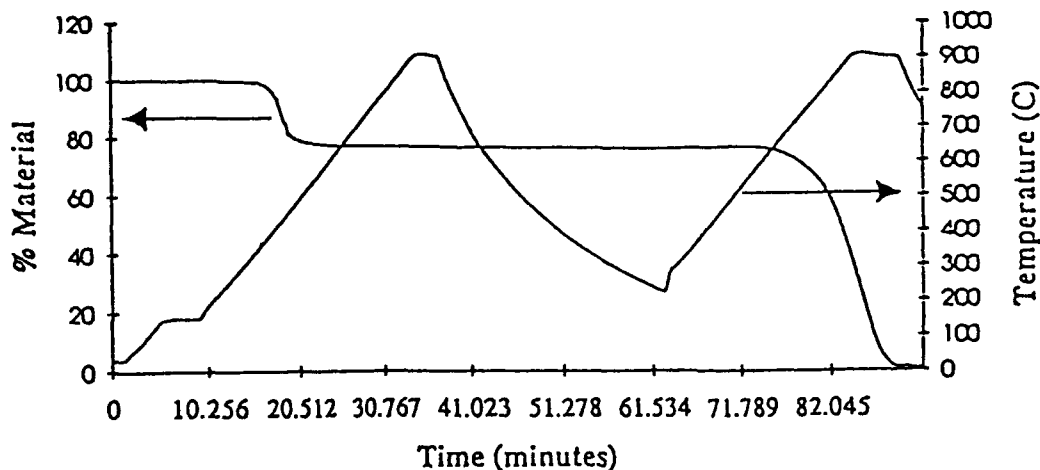

Figure 17. Thermogravimetric Temperature Program. Weight loss (percent of 100), is also Shown. Pyrolysis Occurs between 350 and 500 °C, and Combustion between 600 and 900 °C.

23

The sample is first heated to 150 °C in helium for 4 minutes for drying, then to 900 °C at 30 °C/min for pyrolysis, cooled to 250 °C for 20 minutes, then reheated with a flow of oxygen (20 cm^3) to 900 °C for combustion. A plot of weight loss (as percent in Figure 17) shows pyrolysis occurring between 350 and 500 °C. Sequential gas phase infrared transmission composed of 5 averaged scans and 4 cm^{-1} resolution, were collected every 30 seconds (Figure 18).
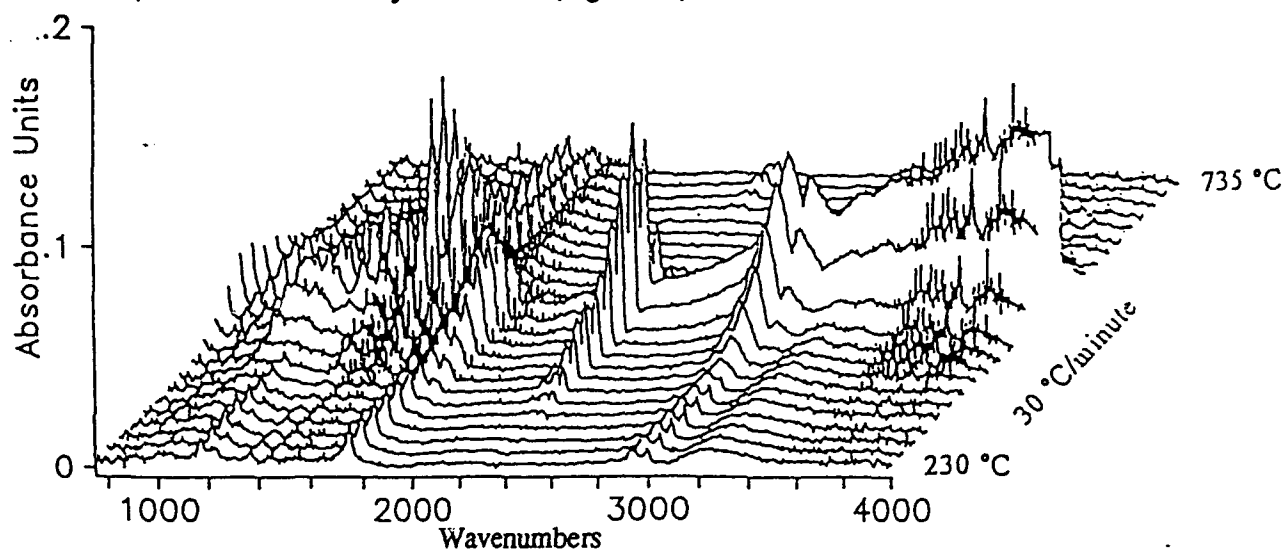
Figure 18. 3-D Spectra of Chemical Species Evolved From Pyrolyzing a Graphite Reinforced Epoxy Resin.

The lowest trace with bands at 1165, 1750, 2940, 2990 and 3240 cm^{-1} represents a highly volatile compound, such as a mold release agent. The band at 1750 is characteristic of stearate compounds as demonstrated by the near perfect spectral match of methyl stearate in Figure 19. Indeed, glycerol tristearate is used as a mold release agent.
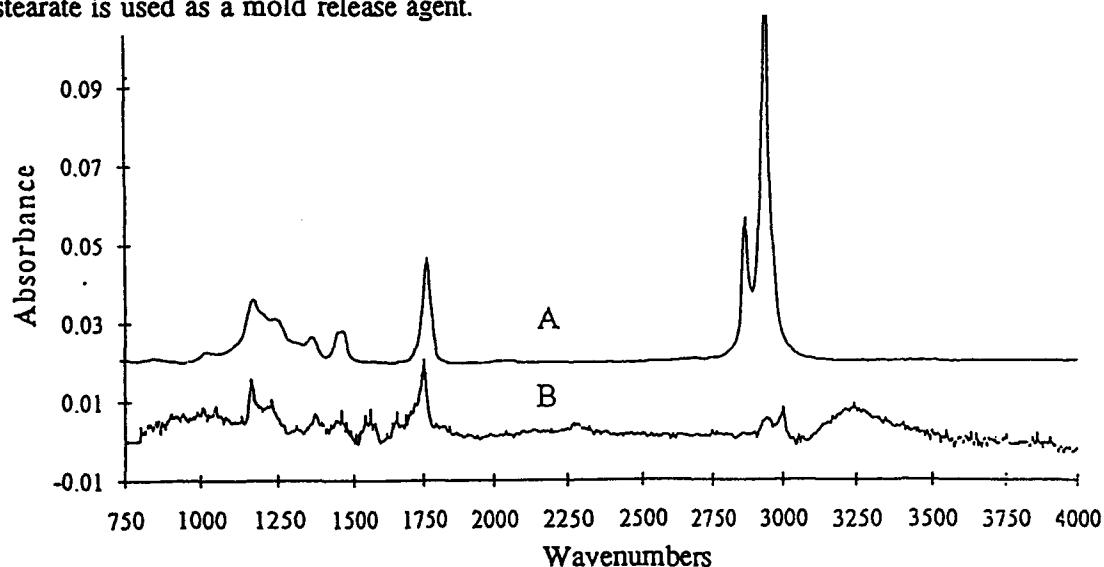
Figure 19. Comparison of Infrared Spectra for A) Methyl Stearate and B) the First Evolved Chemical Species Due to Pyrolysis of Novolac Based Composite.

24

Subtraction of this spectrum from subsequent spectra allows identifying the next species to evolve. It also allows determining the evolution rate of each species. By employing this method, five steps of chemical evolution (one or more chemical species per step) occur during pyrolysis (Figures 20 and 21). The second step is represented by the evolution of an isocyanic acid (sharp band at 2280 cm^{-1}), possibly the product of pyrolysis of either a Novolac functionality or dicyandiamide used for curing. The next step results in bands at 1060, 1800, 2875 and 2945 cm^{-1}. Although an exact chemical identification of this species was not obtained, the 1060 cm^{-1} band could be assigned to a silicon oxide mode, indicating the presence of a siloxane fiber coupling agent. The species evolved in the fourth step is easily assigned to the epoxy resin as demonstrated by comparing the spectral features to uncured epoxy resin presented in Figure 4. However, there are significant bands at 1310, 1625, and 3425 cm^{-1} indicating either an amine or hydroxyl substituted phenyl group. This may represent unreacted or a pyrolyzed by-product of a crosslinking agent. Furthermore, considerable CO_2 and H_2O are generated during this step. Finally, the species evolved in the last step has a sharp band occurring at 713 cm^{-1}, and is assigned to hydrogen cyanide (not shown), again indicating the presence of a cyanide functionality.

Examination of the evolved data clearly show composite thermal degradation starting at below 200 °C with significant degradation at above 350 °C, beyond which catastrophic failure of the composite might be expected. It also suggests heating samples to these temperatures to characterize this failure.
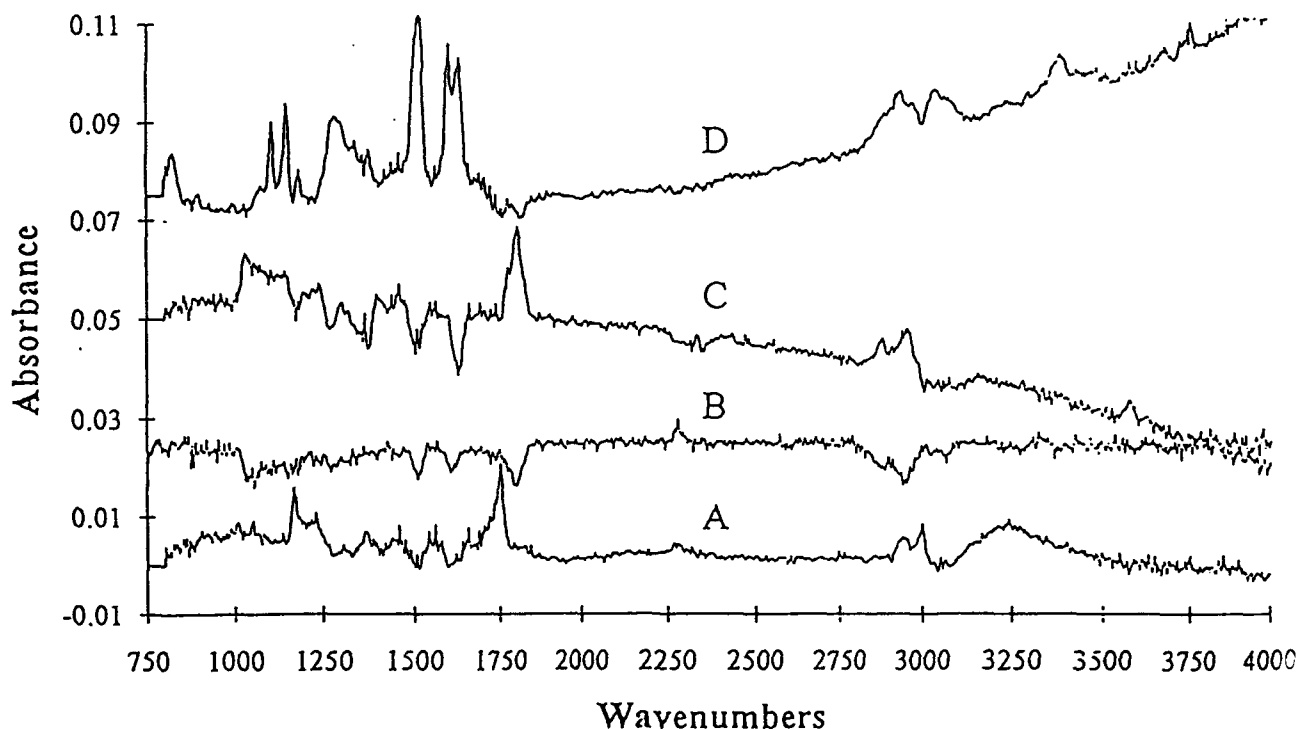

Figure 20. Infrared Spectra of the First Four Evolved Chemical Species Due to Pyrolysis of Graphite/Epoxy Composite. A) 280, B) 340, C) 400, and D) 475 °C.
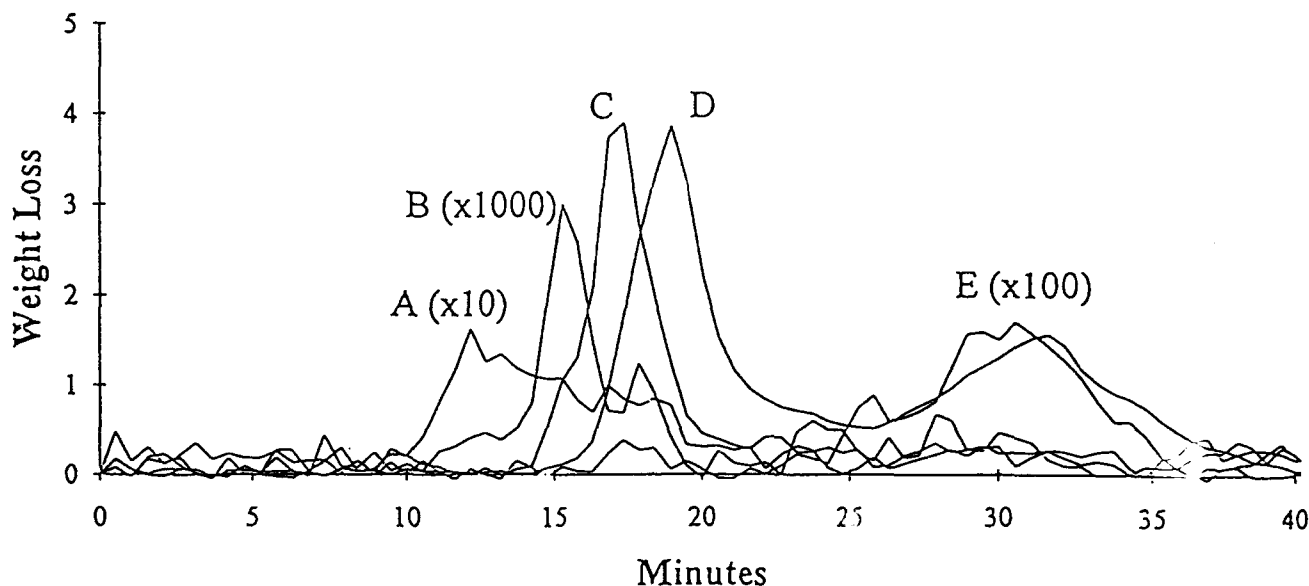
Figure 21. Evolution Rates for Five Evolved Chemical Species Due to Pyrolysis of Graphite/Epoxy Composite. Letters Correspond to Spectra in Figure 20, E) is at 790 °C.

3.c.3. Composite #2 = Kevlar Reinforced Epoxy Resin (Hexcel F161)

Employing conditions previously described, the TG/plus instrument was used to pyrolyze composite #2 and #3. A 5 mg sample of composite #2 was heated according to the same temperature pyrolysis program for Composite #1. Weight loss occurs in three stages of increasing magnitude (Figure 22). The first occurs at 333 °C, the second at 445 °C, and the third at 617 °C (determined from second derivative). Sequential gas phase infrared transmission spectra composed of 5 averaged scans and 4 cm^{-1} resolution, were collected every 30 seconds (Figure 23). Selected spectra associated with these weight losses were extracted from Figure 23 and presented in Figure 24. These spectra represent various chemicals evolving during degradation. Preliminary analysis suggests evolution of: 1) a mold release or fiber coupling agent at 333 °C, 2) degradation products of the epoxy matrix at 445 °C, and 3) a degradation product of the Kevlar reinforcement fiber at 617 °C (as supported by transmission infrared spectra, see below). The 445 °C spectrum is composed of a degradation product closely related to p-hydroxy phenyl 2-butone probably the resin polymer backbone (see Figure 25) and an amine probably due to a curing agent (note bands at 2200 and 3500 cm^{-1}).
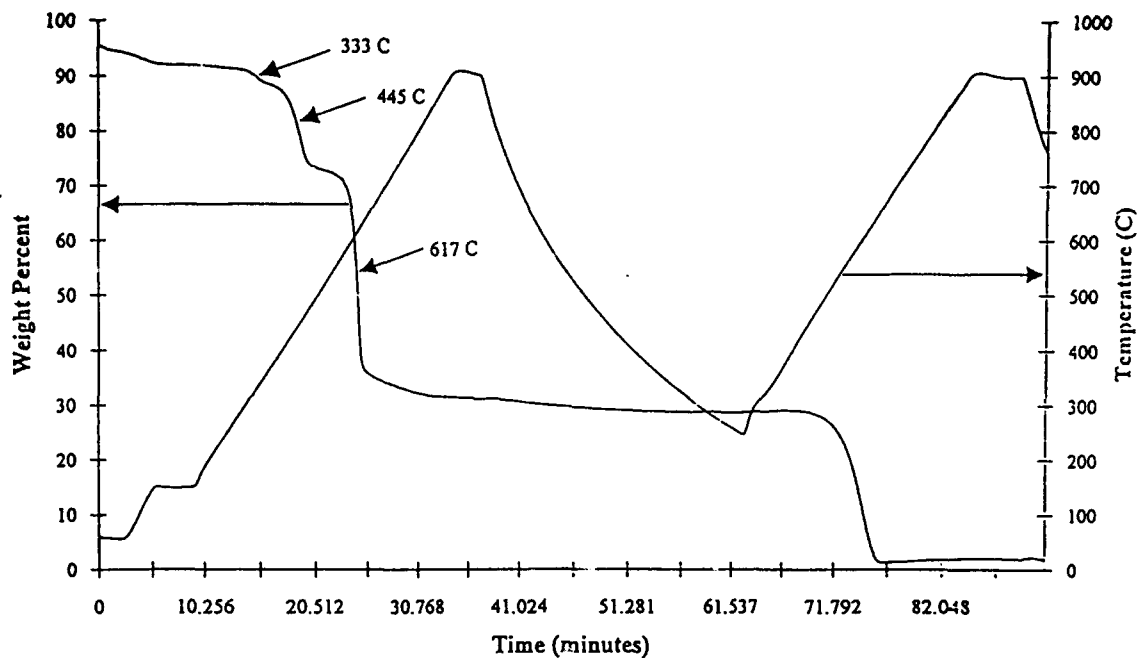
26

Figure 22. Thermogravimetric Temperature Program and Weight Loss for Composite #2. Pyrolysis Occurs Between 300 and 650 °C, While Combustion Occurs Between 450 and 650 °C.
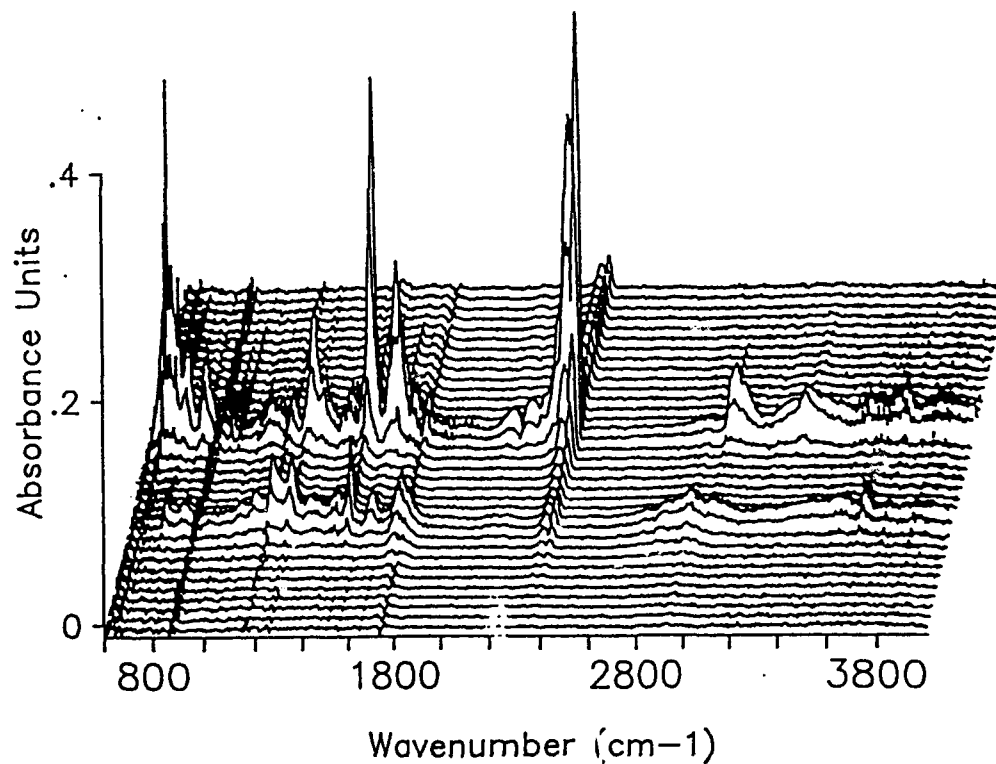

Figure 23. 3-D Spectra of Evolved Chemical Species During Pyrolysis for Composite #2.
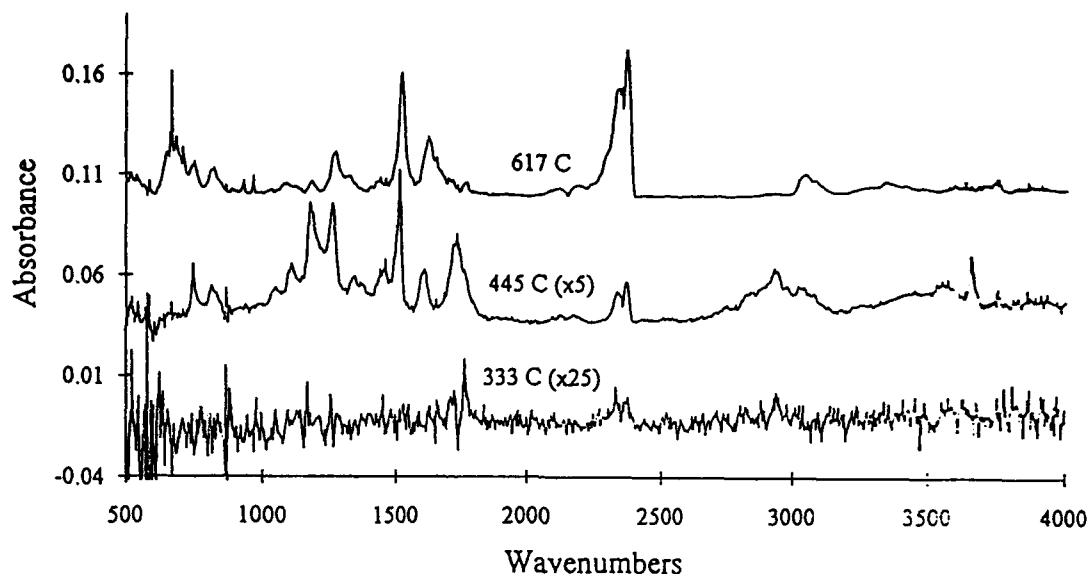
27

Figure 24. Infrared Spectra of Evolved Species Associated with Weight Loss. Spectra Were Artificially Scaled and Offset for Presentation Purposes.
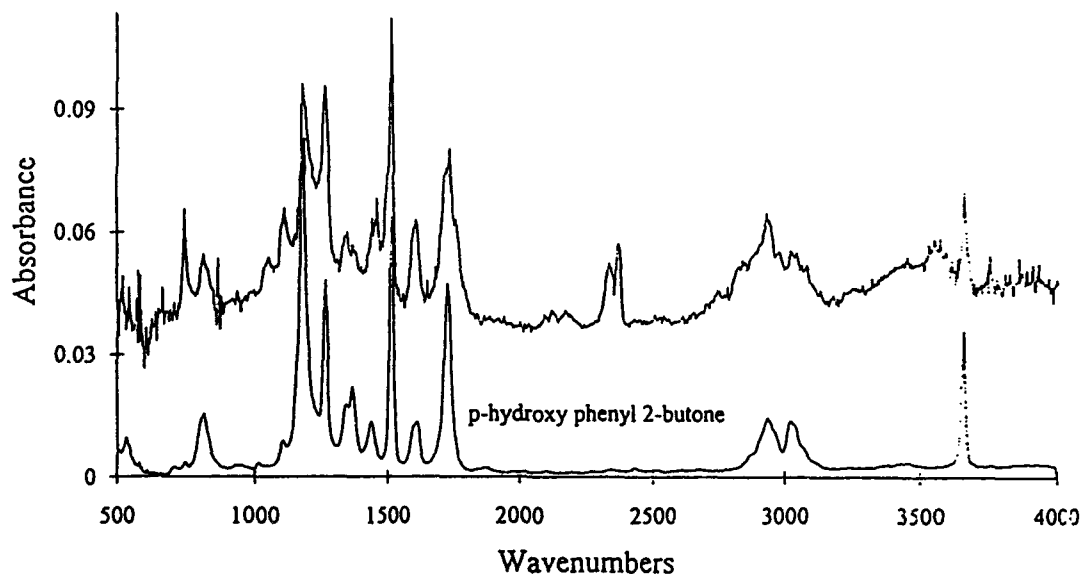

Figure 25. Comparison of Spectra for the Second Stage of Pyrolysis and p-Hydroxy Phenyl 2-Butone.

3.c.4. Composite #3 = Graphite Reinforced Polyimide (PMP-15)

Our initial Composite #3 (obtained from UT-PW), presumed to be a polyimide, was subjected to thermogravimetric analysis. However, the evolved spectrum, nearly identical to Composite #1, clearly identified this compound to also be an epoxy resin based composite.

Employing conditions previously described, the TG/plus instrument was used to pyrolyze the composite obtained from Case Western Reserve University. A 3.9 mg sample was heated according to the temperature pyrolysis program in Figure 17. Sequential gas phase infrared transmission spectra

composed of 5 averaged scans and 4 cm⁻¹ resolution, were collected every 36 seconds (Figure 26). Selected spectra associated with these weight losses were extracted from Figure 26 and presented in Figure 27. These spectra suggest two chemicals evolve during degradation. For example, note the relative intensity of the 1714 and 1744 cm⁻¹ doublet. It is also noted that carbon monoxide (2110, 2180 cm⁻¹ doublet) evolves at higher temperatures.
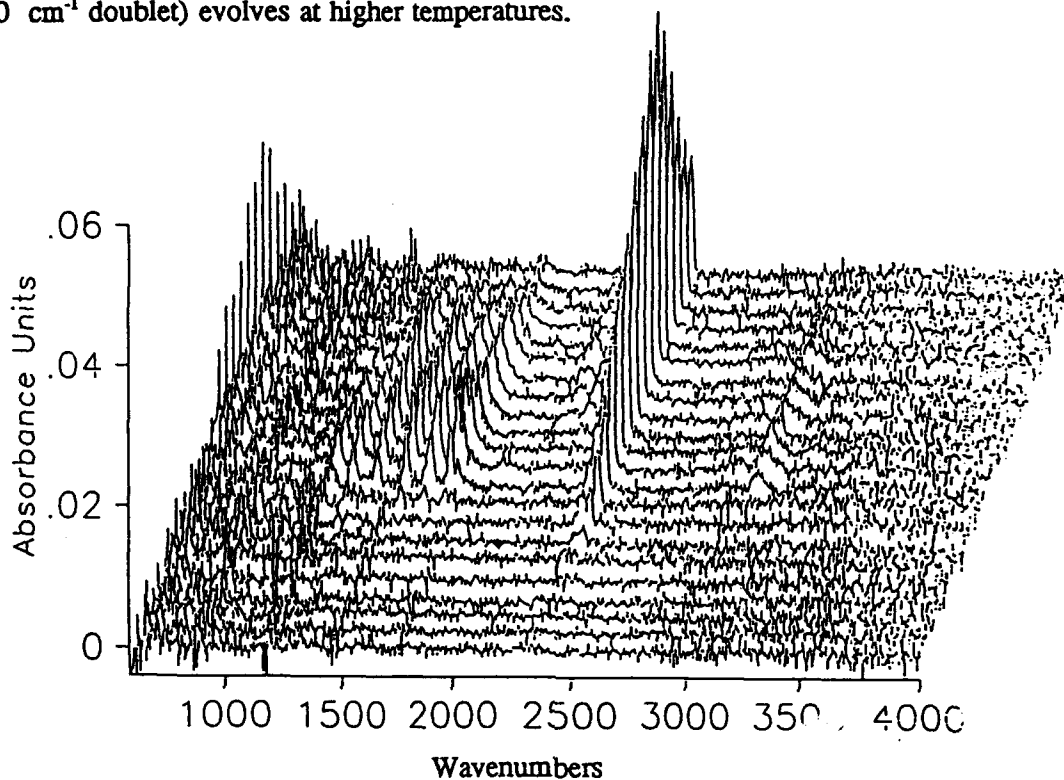
Figure 26. 3-D Spectra of Evolved Chemical Species During Pyrolysis of Composite #3.
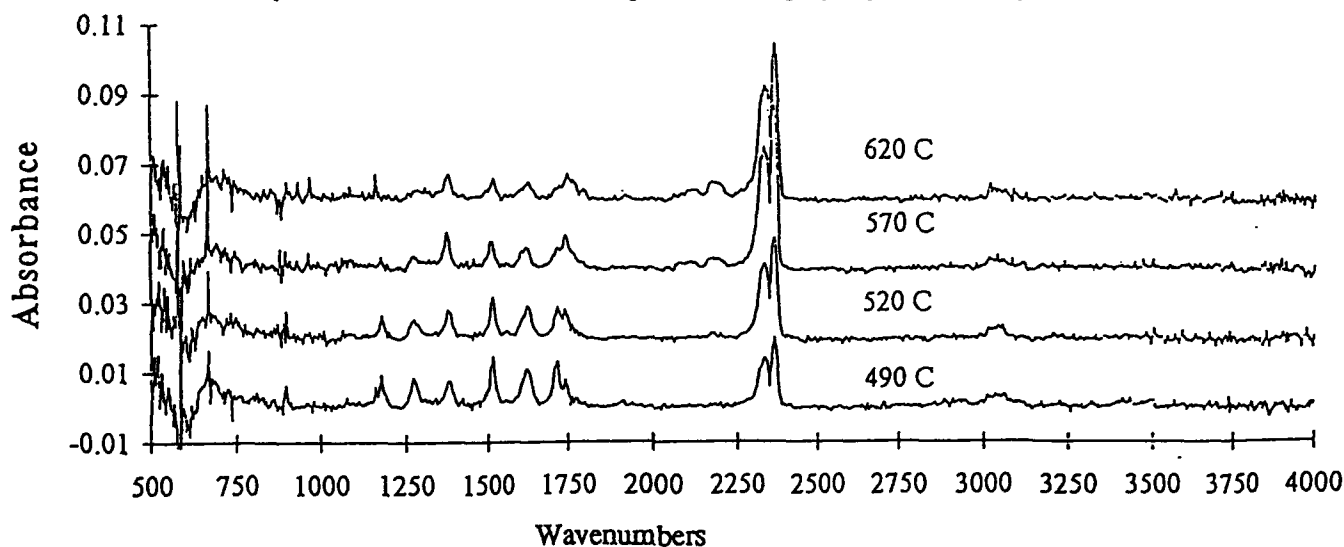
Figure 27. Gas Phase Infrared Spectra of Evolved Species at Selected Temperatures from Composite #3. Spectra were Artificially Offset for Clarity.

3.c.5. Chemical Degradation

Attempts to extract the polymers with various solvents proved futile, as did reactions with hydrochloric acid. For this reason, the samples (Composite #1 and #2) were ground into fine powders and placed between KBr plates for FT-IR transmission measurements. The spectra were obtained on a Nicolet model 7199 and baseline corrected (Figure 28). A number of vibrational bands for each composite are readily observed. Both spectra contain two broad absorptions, one from 800 to 1600 cm^{-1} (centered at 1300 cm^{-1}), and one from 2800 to 3600 cm^{-1}, and are attributed to graphite.
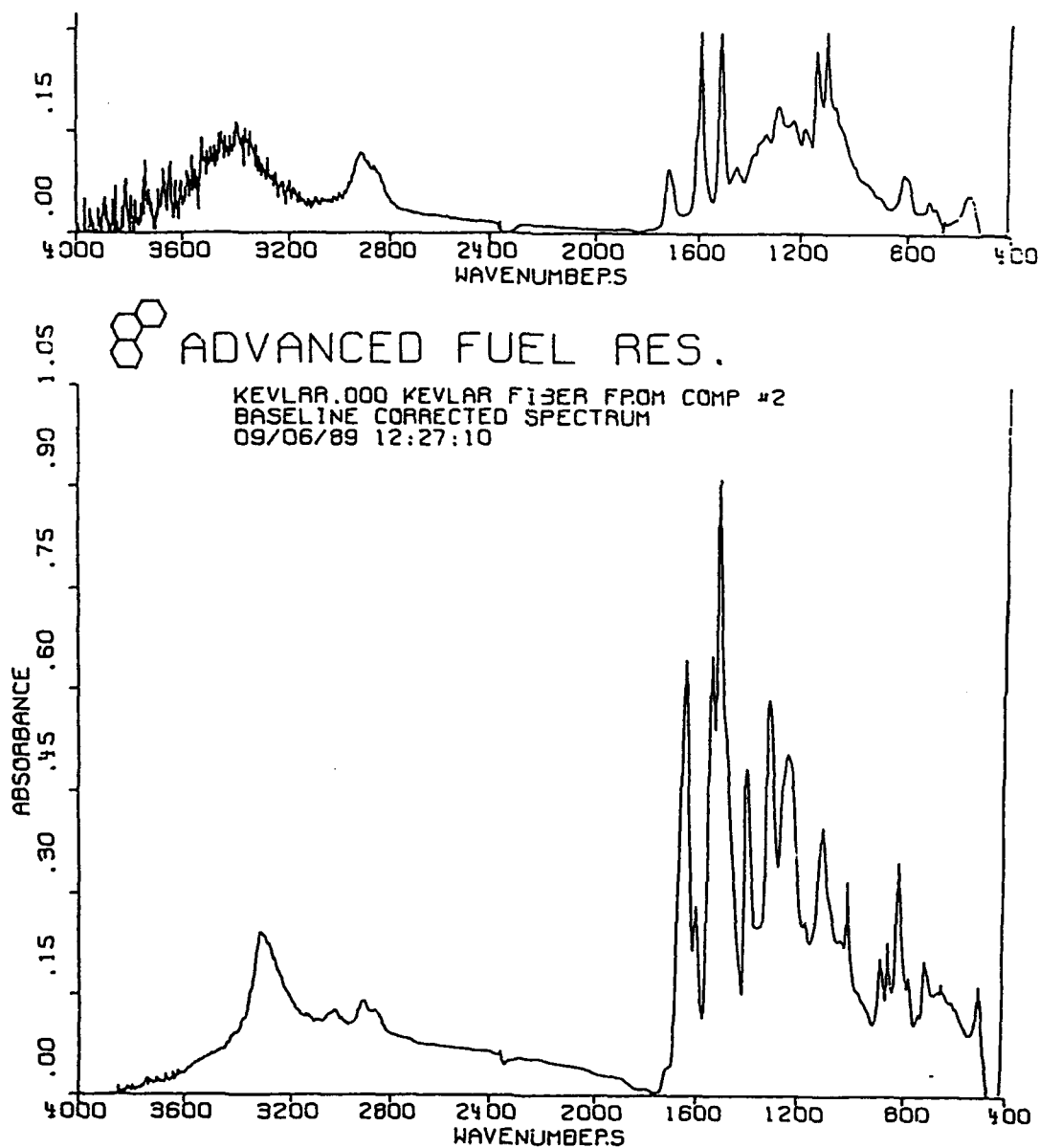

Figure 28. Transmission Infrared Spectra of A) Graphite/Epoxy Composite and B) Kevlar/Epoxy Composite Powders. Collection on a Nicolet model 7199, 4 cm^{-1} Resolution, 100 Scans.

3.d. Task 3 - Raman Spectra

3.d.1. Diffuse Reflectance Infrared Spectra

Previously, we demonstrated the ability of diffuse reflectance (DR) spectroscopy to characterize composites. These spectra were simply baseline corrected, however, improved spectral analysis is obtained by converting the spectra to Kubelka-Munk intensity units as described in literature.[20] Figure 29 shows the DR spectra of the three composites prior to treatment. Tables 2 and 3 list the principle vibrational peaks observed.
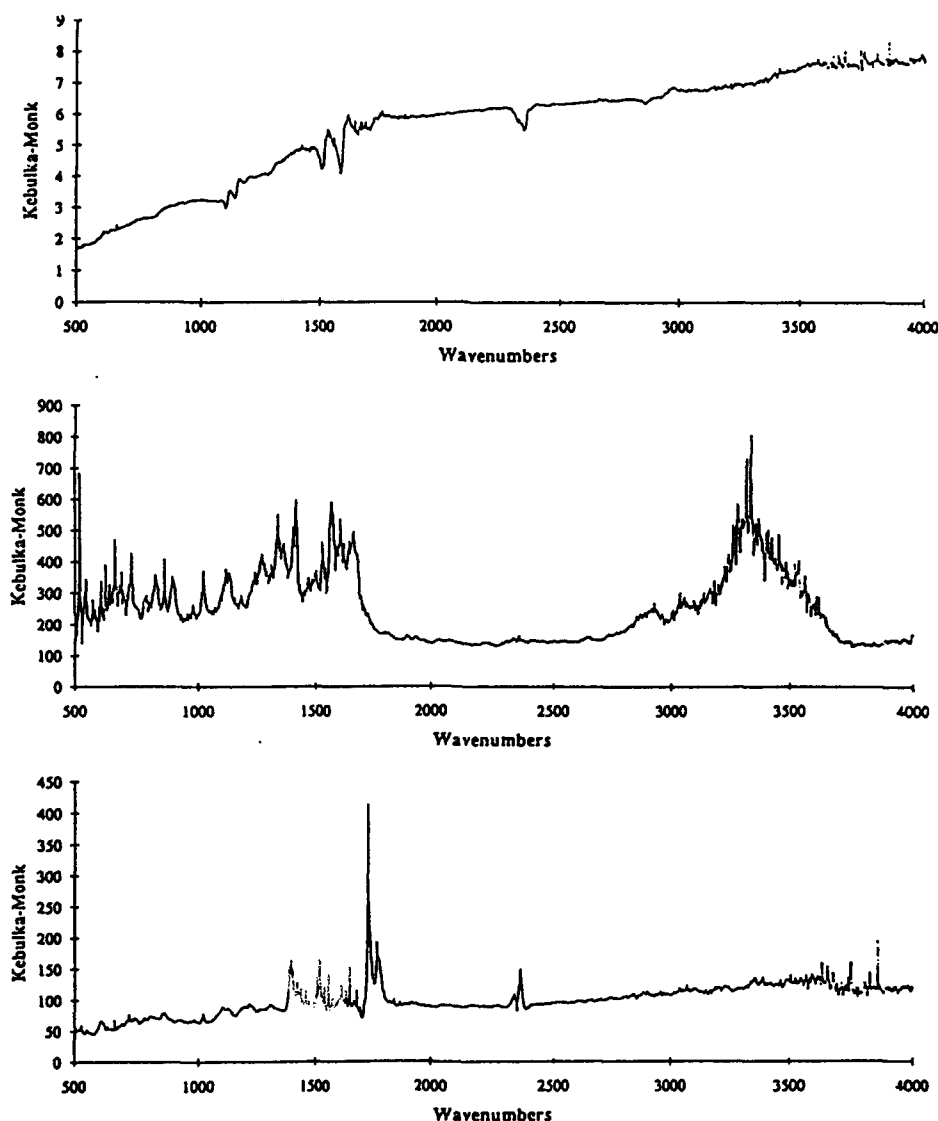

Figure 29. Diffuse Reflectance for Untreated A) Graphite/Epoxy, B) Kevlar/Epoxy, and C) Graphite/Polyimide Composites. Note Kubelka-Munk Units.

Table 2. Graphite/Epoxy Composite with Literature Epoxy Resin Infrared Spectral Peak Assignments

Peak or band, cm^{-1}	Assignment
3450-3500	vO-H
3050	Aromatic C—H stretch
3038	Epoxide CH, C—H
2998	Epoxide methylene C—H
2928	Ether methylene C—H assym. stretch
2840	Ether methylene C—H sym. stretch
2872	Methyl C—H sym stretch
2962	Methyl C—H assym. stretch
1700-2200	Aromatic combination bands
1605	
1580	
1508	Aromatic C=C bands
1560	
1430	Epoxide δ_{C-H}
1410	Epoxide/etherδ_{C-H}
1382	Methyl δ_{C-H} sym. defeformation
1360	Ether methylene δ_{C-H}
1345	Epoxide methylene δ_{C-H}
1290-1310	ϒCH$_2$, aromatic δ_{C-H}, δ_{-OH}
1230-1260	Aromatic ether aryl C—O, epoxide C—O—C
1185	Aromatic δ_{C-H}, (in plane)
1105-1135	Aromatic δ_{C-H}, C(CH$_3$)$_2$ skeletal
1038	Aromatic δ_{C-H}, aromatic ether alkyl C—O
1010	Aromatic δ_{C-H}
915-920	Epoxide deformation
862	Epoxide deformation
830	Aromatic δ_{C-H} out-of-plane
810	C(CH$_3$) skeletal
750-780	CH$_2$ skeletal
Lower peaks	Assignment unclear

Table 3. Observed DR and Raman Band Intensities for Graphite/Epoxy, Kevlar/Epoxy, and Graphite/Polyimide

Graphite/Epoxy	Kevlar/Epoxy		Graphite/Polyimide
DR	DR	Raman	DR
1082	668	790 w	531
1122	732 s	915 w	555
1160 s	827 s	1107 w	614
1199 s	865 s	1186	638
1257 w	896 s	1281 s	667
1315	980 w	1333 vs	726
1421	1020	1521	750
1468	1113	1573 w	786
1535 s	1132	1615 vs	811
1623 s	1180	1653 vs	863
1742 br	1272	3078 br, w	1021
2975 br	1308		1098
3518	1337 s		1120
3621	1360		2172
3733	1400		1273
3890	1410		1302
3991	1470		1393
	1496 br		1429
	1530 s		1519
	1570 vs		1615
	1611 s		1740
	1662 s		1780
	2908 br		
	3052 br		
	3293 s		
	3327 vs		
	3417		

br = broad; s = strong; vs = very strong; w = weak

The DR spectra of Composite #1 (Graphite/Epoxy) heated to 250, and 340 °C for 10 minutes, boiled in water for 10 hours, and exposed to ultraviolet radiation for 100 hours are shown in Figures 30, 31, and 32, respectively. For both the heated and UV exposed samples, a significant loss in band intensity occurs with increased exposure, as expected. Surprisingly, band intensities remain nearly constant for moisture exposure. This suggests that neither water inclusion or reaction takes place under these conditions.
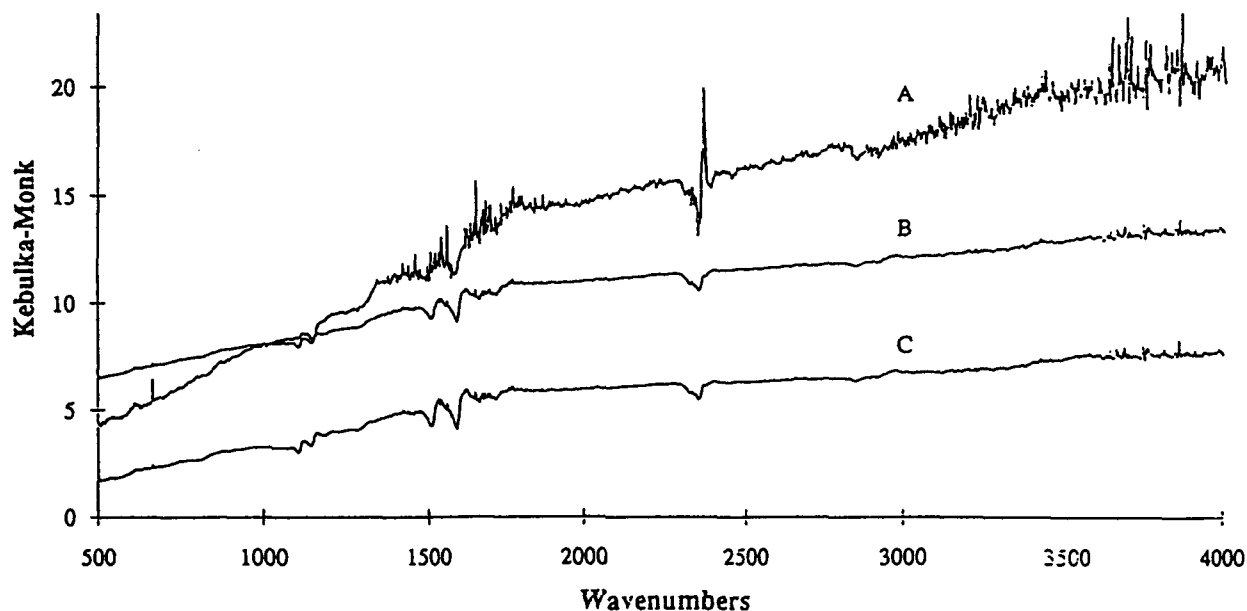
Figure 30. Diffuse Reflectance Spectra Converted to Kubelka-Munk Units of Graphite/Epoxy Composites at C) Room Temperature, B) 250 °C, and A) 340 °C.
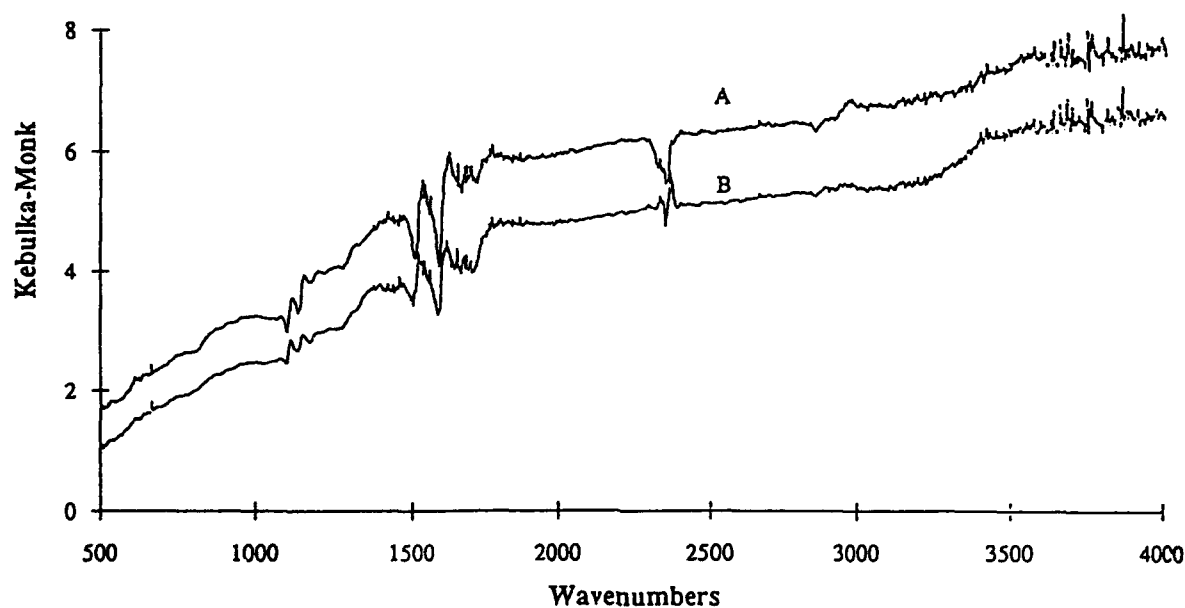
Figure 31. DR Spectra in KM Units for Graphite/Epoxy Composites A) Unexposed and B) Exposed to UV Radiation for 100 Hours.
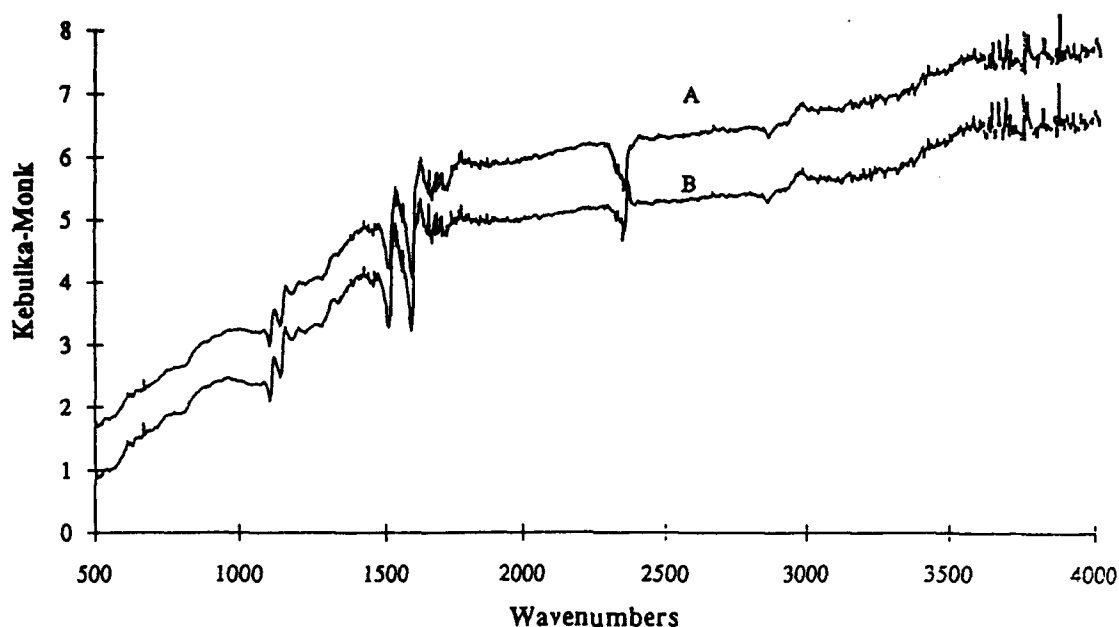
Figure 32. DR Spectra in KM Units for Graphite/Epoxy Composites A) Unexposed and B) Boiled in Water for 10 Hours.

The DR spectra of Composite #2 (Kevlar/Epoxy) heated to 200, and 380 °C for 10 minutes, boiled in water for 10 hours, and exposed to ultraviolet radiation for 100 hours are shown in Figure 33, 34, and 35, respectively. A number of the bands increase significantly as the sample is heated (200 °C), but disappear at higher temperatures. This is interpreted as removal of the epoxy layer revealing the underlying Kevlar fibers, thus gaining signal intensity before they subsequently degrade. This is supported by comparison of our Kubelka-Munk spectrum to literature,[20] which shows excellent agreement (Figure 36).
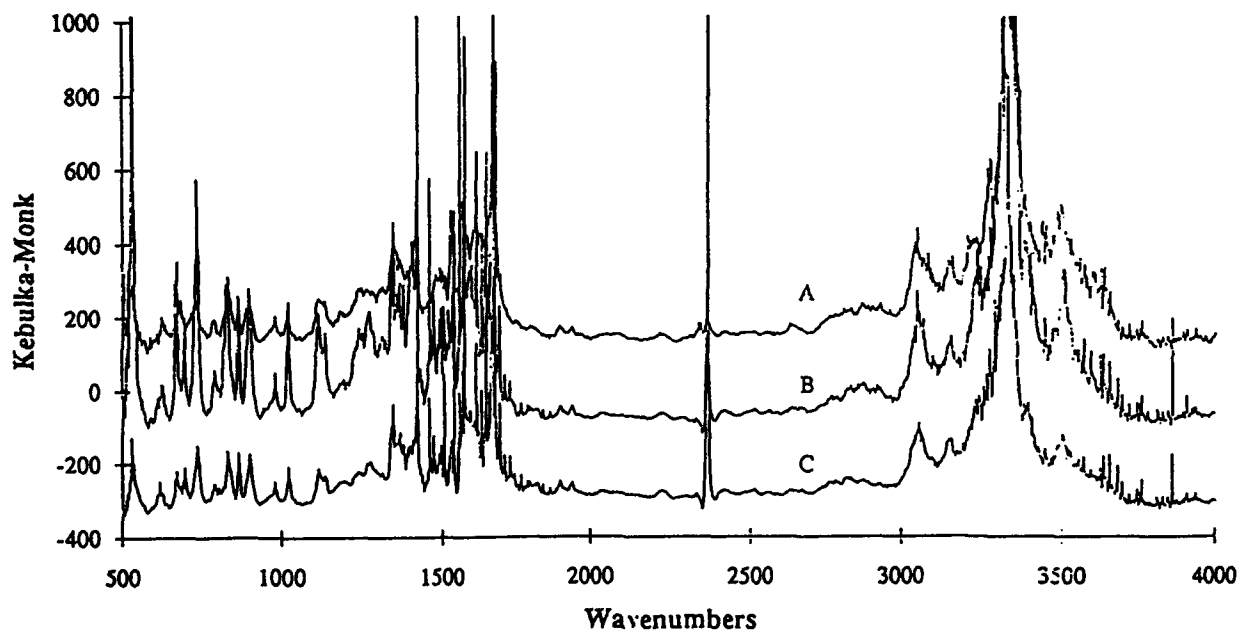
Figure 33. DR Spectra in KM Units for Kevlar/Epoxy Composites at A) Room Temperature, B) 200 °C, and C) 380 °C. Apparent Noise from 1400 to 1700 and 3200 to 3800 cm^{-1} is due to water vapor in the measurement beam path.
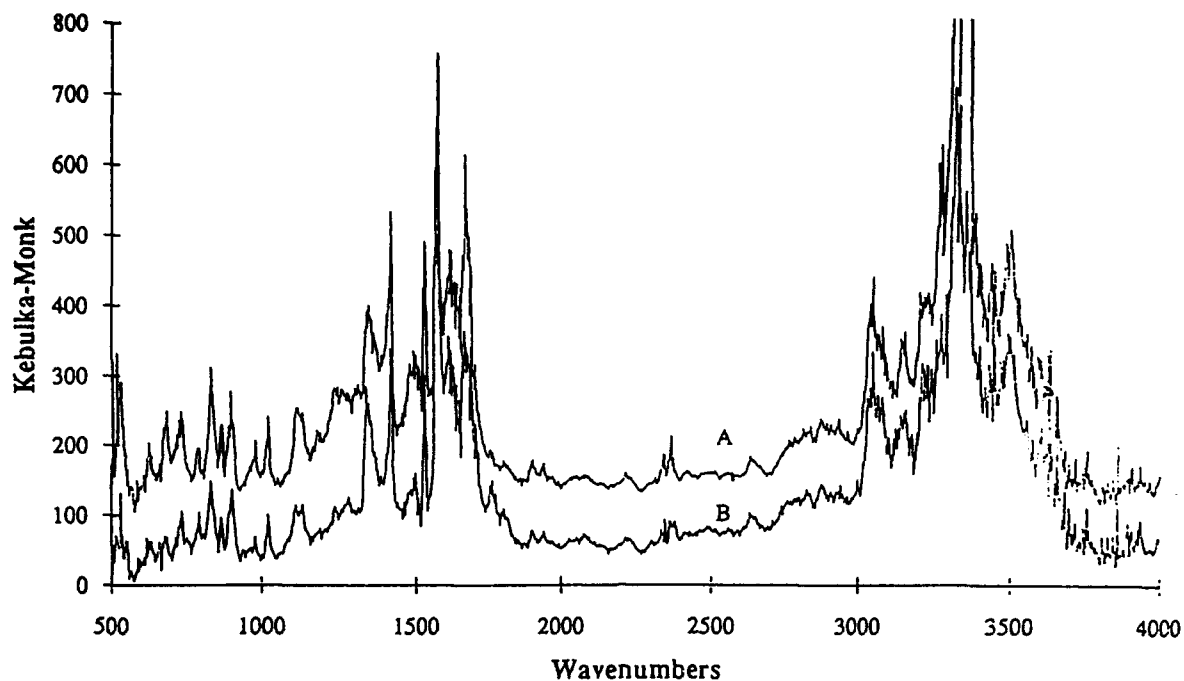
Figure 34. DR Spectra in KM Units for Kevlar/Epoxy Composites A) Unexposed and B) Exposed to UV Radiation for 100 Hours.
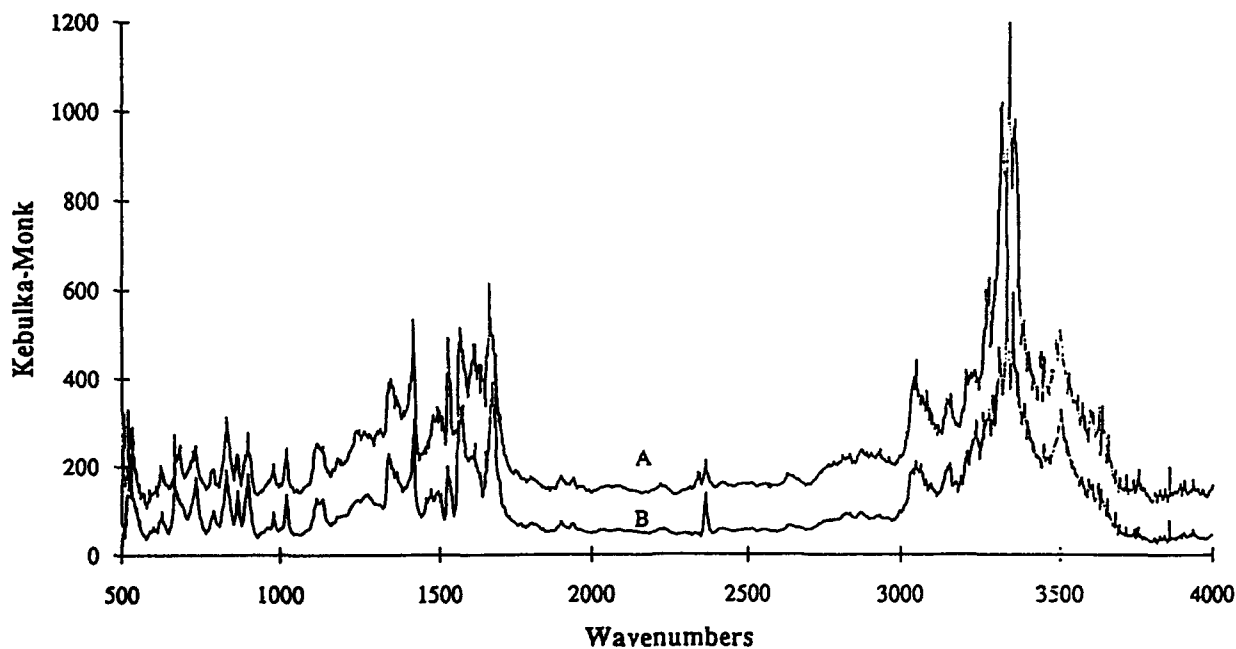
Figure 35. DR Spectra in KM Units for Kevlar/Epoxy Composites A) Unexposed and B) Boiled in Water for 10 Hours.

Again very little degradation, if any, occurs due to exposure to boiling water. Exposure to UV radiation does result in a moderate decreased band intensities. Furthermore, inspection of the UV exposed sample reveals a loss in the quality of the Kevlar fibers, suggesting degradation. The epoxy filler may also be degraded as suggested by the measurements on Composite #1.
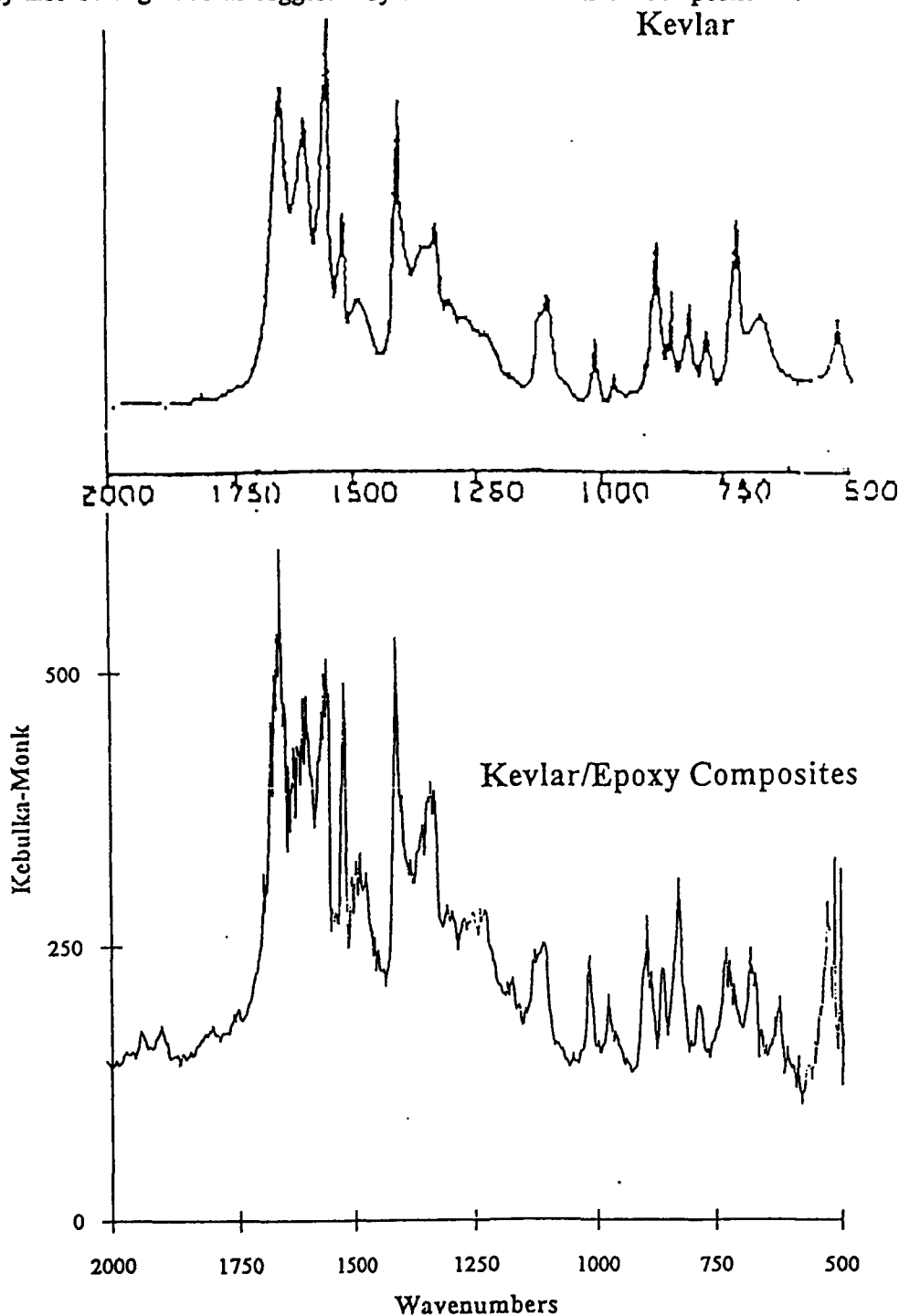
Figure 36. DR Spectra in KM Units for A) Kevlar from Literature[20] and B) Kevlar/Epoxy Composites Measured Here.

The DR spectra of Composite #3 (Graphite/Polyimide) heated to 250, and 500 °C for 10 minutes, and exposed to ultraviolet radiation in the presence of 40% oxygen for 100 hours are shown in Figure 37, and 38, respectively. For both the heated and UV exposed samples, a significant loss in band intensity occurs with increased exposure. Indeed, there is a marked decrease in the 1740 cm^{-1} imide band suggests significant UV enhanced chemical degradation. It should be noted that visual inspection of the UV exposed sample shows no sign of degradation. Again, no changes are observed for samples exposed to boiling water.

Figure 37. DR Spectra in KM Units for Graphite/Polyimide Composites at A) Room Temperature, B) 250 °C, and C) 500 °C. Apparent Noise from 1400 to 1700 and 3200 to 3800 cm^{-1} is due to water vapor in the measurement beam path.

Figure 38. DR Spectra in KM Units for Kevlar/Epoxy Composites A) Unexposed and B) Exposed to UV Radiation in 40% Oxygen for 100 Hours.
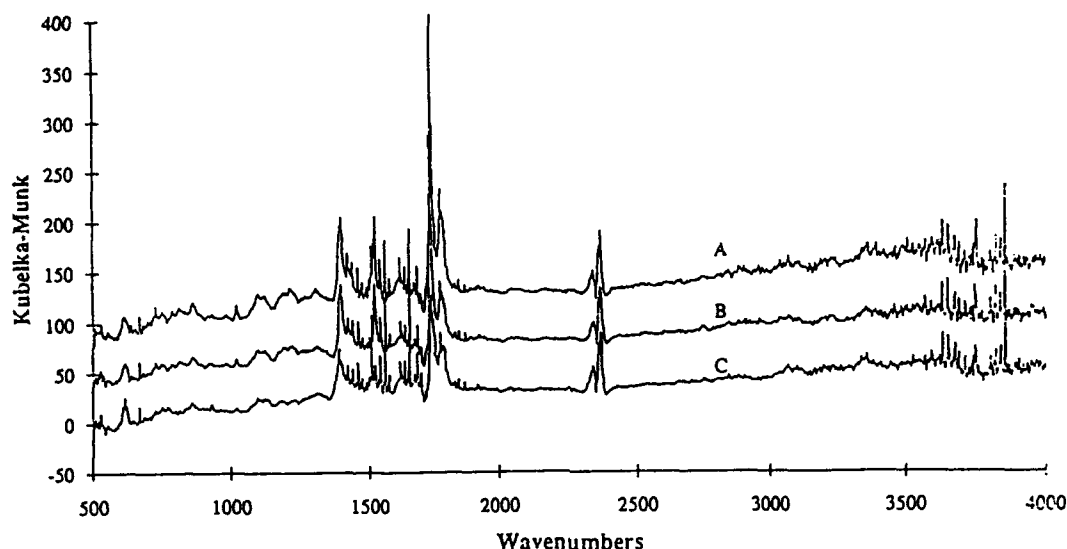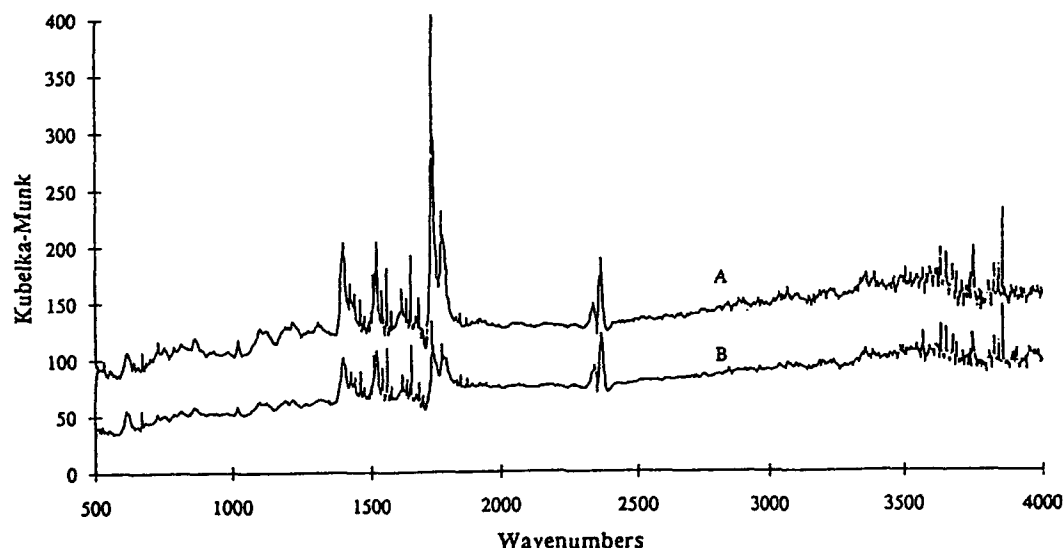
38

3.d.2. FT-Raman Spectra

The design improvements to the FT-Raman system described in this report have made collection of spectra for the Kevlar/Epoxy composite straight forward, as shown in Figure 39. A comparison to an FT-Raman spectrum of Graphite/Epoxy (dominated by epoxy bands) suggest the former spectral features are due to the Kevlar fibers. This interpretation is consistent with the DR infrared spectra. Raman spectra for the Kevlar/Epoxy composite were also obtained at several excitation wavelengths using several CCD based Raman spectrometers; Dilor (10 mW of 514.5 nm, Ar+ laser), Oriel (10 mW of 632.8 nm, HeNe laser), and Chromex (30 mW of 785 nm, diode laser). Although all instruments yield good signal to noise, visible excitation results in a sloping baseline probably due to sample fluorescence (Figure 40).
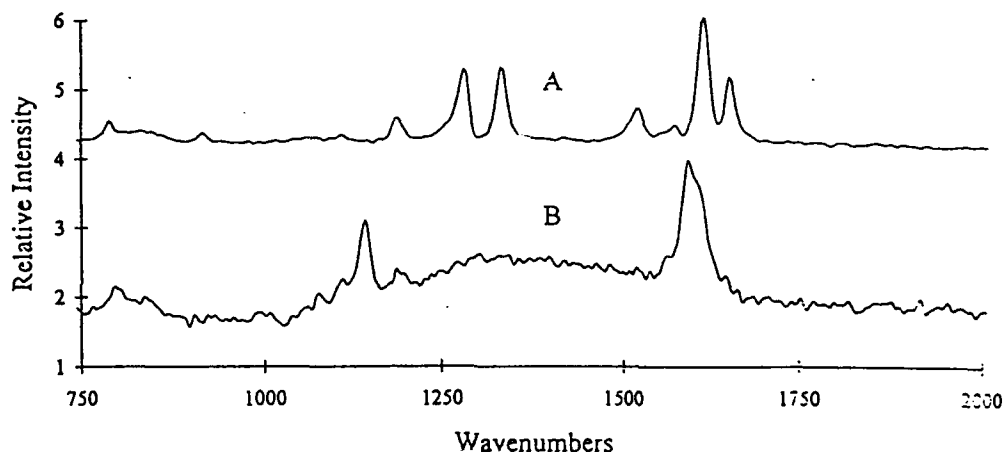
Figure 39. A) FT-Raman Spectra of Composite #2 using AFR Designed System. Conditions: 0.43W of 1064 nm, 1x6 365 µm fiber probe at 2mm from 5 Hz spun sample, 8 cm^{-1} resolution, 100 averaged scans. FT-Raman Spectrum of Composite #1 Included for Comparison Using Nicolet FT-Raman 910. Conditions: 0.10W of 1064 nm, 4 cm^{-1} resolution, 100 averaged scans.
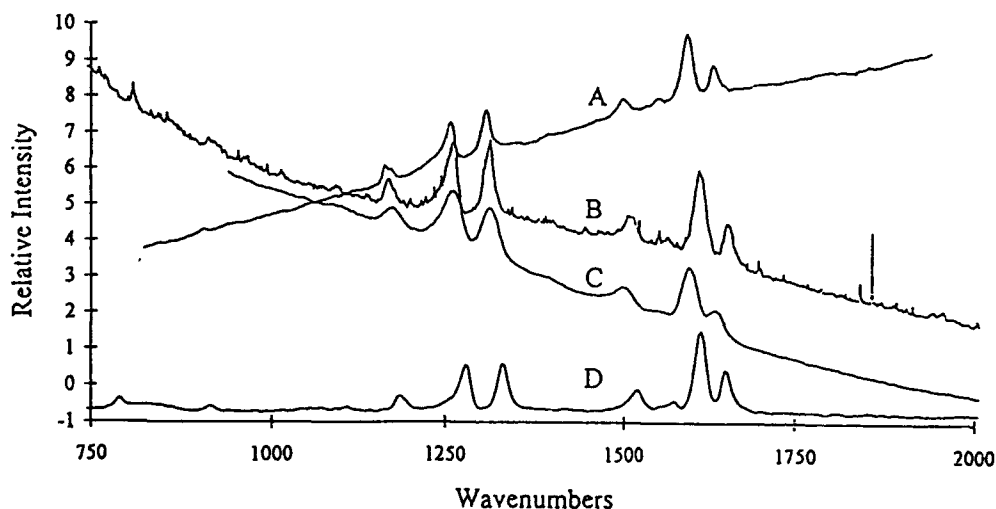
Figure 40. Comparison of Raman Spectra of Composite #2 at Different Laser Excitation Wavelengths. A) Dilor, 10 mW of 514.5 nm, 50 averaged scans; B) Oriel, 10 mW of 632.8 nm, 60 scans; C) Chromex, 30 mW of 785 nm, 50 scans; D) AFR System (see Figure 39).

FT-Raman spectra were also collected for the environmentally treated composite #2 samples, and are shown in Figures 41-43. Since samples are clearly heterogeneous (fiber vs. matrix), the probe was positioned 2 mm above the sample surface. In addition to eliminate possible sample heating from the laser source, they were placed on a rotating stage (Sprite fan, ComAir/Rotron) and spun at 5 Hz. All spectra consist of 0.48W at the sample, 8 cm^{-1} resolution, and 100 averaged scans. The thermally treated samples showed a significant rise in the baseline for samples exposed to higher temperatures. This is attributed to broadband re-emission of the laser energy being absorbed by matrix or fiber degradation products. Furthermore, the overall band intensities decrease for higher temperature exposures. Exposure of composite #2 to ultraviolet irradiation (40% oxygen) or boiling water yielded no relative spectral intensity changes. Changes in absolute spectral intensity are likely due to changes in sample positioning or laser intensity.
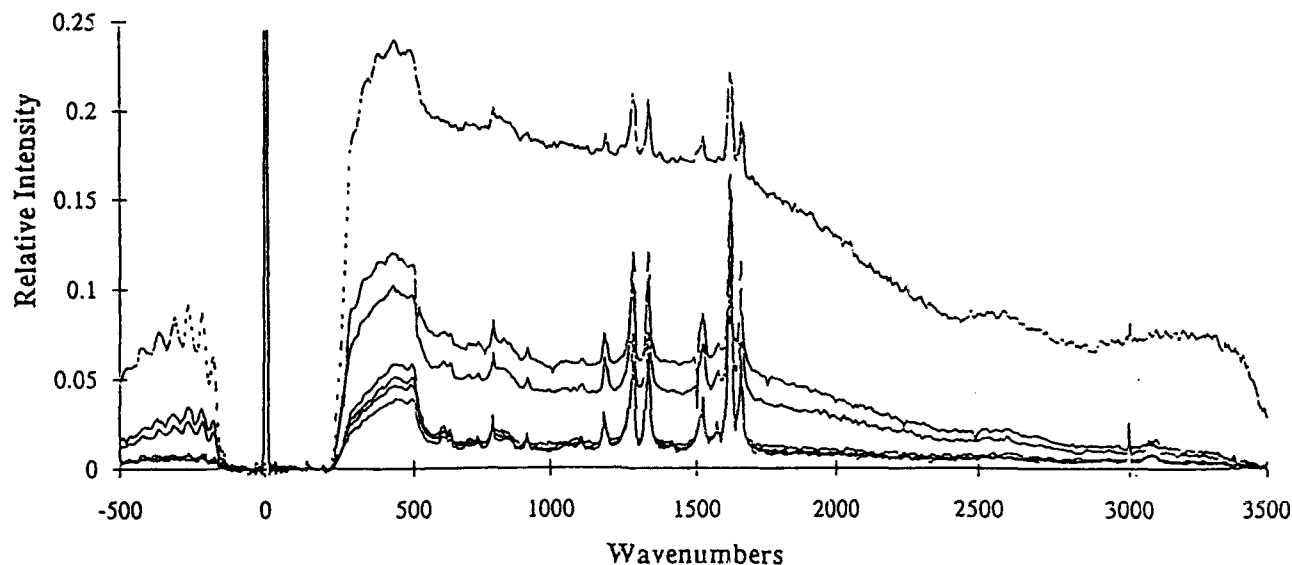

Figure 41. FT-Raman Spectra of Heated Kevlar/Epoxy Composite Samples. Conditions as in Figure 39. In Ascending Order: 25, 100, 200, 300, 340, 360, 380, and 400 °C.
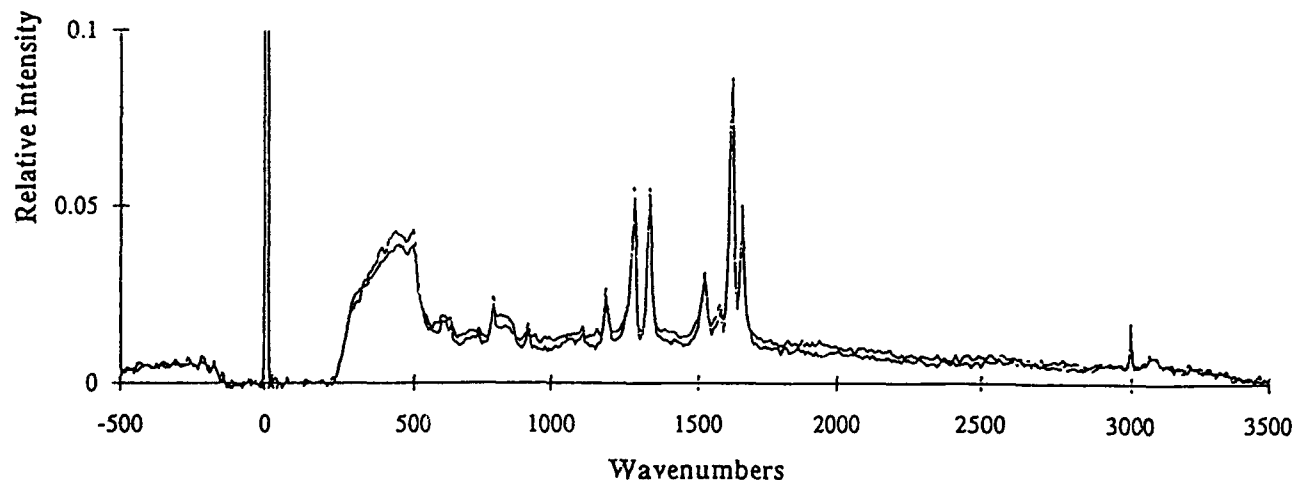
Figure 42. FT-Raman Spectra of UV Exposed Kevlar/Epoxy Composite Samples. Lower Spectrum, Unexposed, Upper Spectrum, 100 Hours in 40% Oxygen.
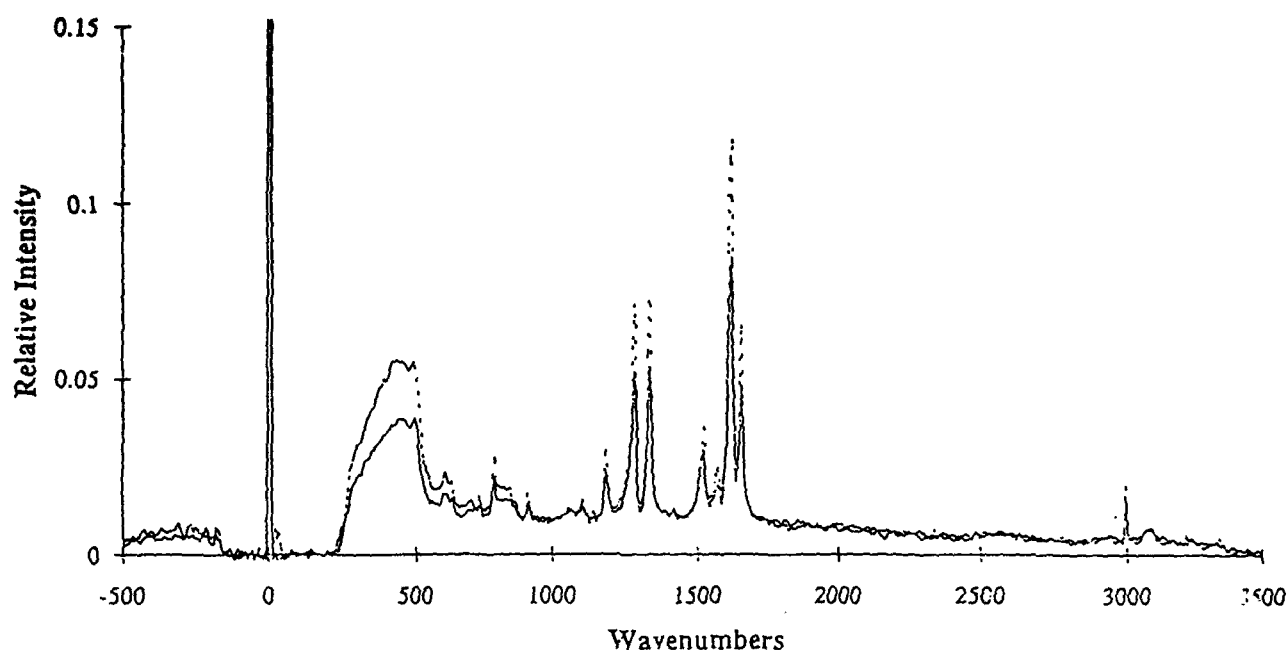
Figure 43. FT-Raman Spectra of Moisture Exposed Kevlar/Epoxy Composite Samples. Upper *Spectrum, Unexposed, Lower Spectrum, Boiled in Water for 10 Hours.*

Preliminary FT-Raman spectra of composite #1 and #3 are shown in Figure 44. Both samples heat easily (even at low laser powers and sample spinning) resulting in broad spectral bands near 3300 cm^{-1}. The low frequency features are due to the silica fiber optics. The fiber probe was also coupled to a lens allowing a tight focus of the laser beam on the sample. This allowed positioning the epoxy "rich" portion of composite #1 in the beam, minimizing contributions from the graphite fibers. Nevertheless, spectra of the epoxy resin bands were still unobtainable. In lieu of these results, as previously reported, FT-Raman spectra were obtained using conventional 180° backscattering sample geometry using a Nicolet system. Figure 45 shows the FT-Raman spectra for heated samples of composite #1.
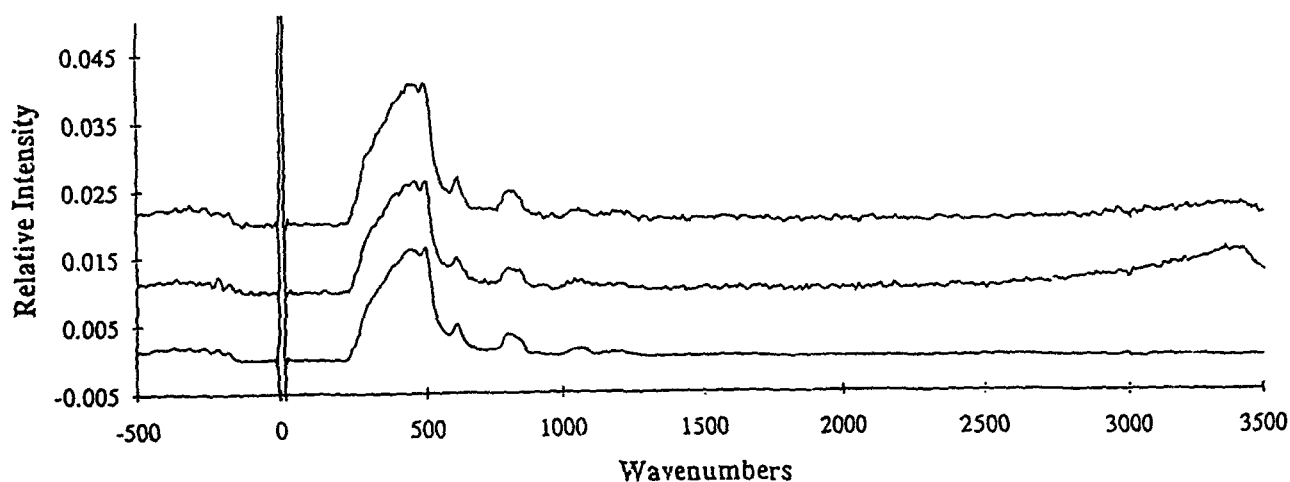
Figure 44. FT-Raman Spectra of Top) Graphite/Polyimide, Middle) Graphite/Epoxy, and Bottom) Gold Mirror. Conditions: 0.1W of 1064 nm, 2mm from 5Hz spinning samples.

41
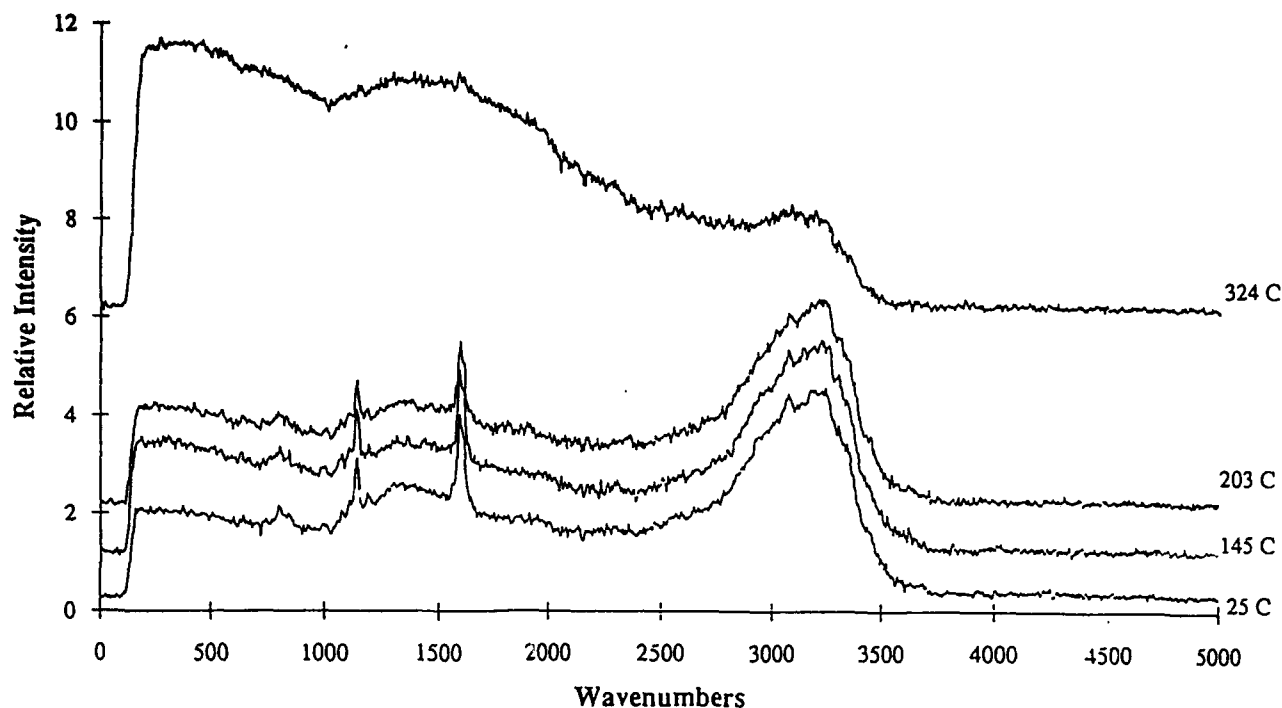
Figure 45. FT-Raman Spectra of Heated Graphite/Epoxy Composite Samples. Temperatures as Shown.

3.e. Task 4 - Mechanical Properties

3.e.1 Three Point Bending Tests

Although these tests were initially to be performed at UT-PW, company restructuring has made this impossible. During the negotiating period, we identified Springborn Laboratories (Enfield, CT) as an alternative. Selected samples were sent to Springborn Laboratories to be mechanically characterized by three point bending tests (Figure 46) using an Instron 1123 universal testing machine to determine failure load, failure strain, flexural strength and flexural modulus. The test results are summarized in Table 4.

Figure 46. Three Point Bending Test Arrangement.

Table 4. Summary of Three Point Bending Tests. DR and Raman Peak Intensities Included.

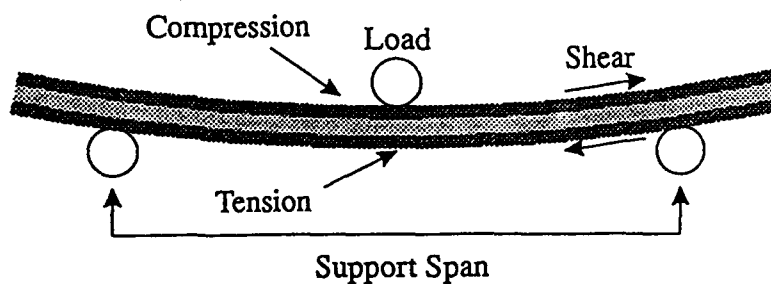| Sample Identificiation	Failure Load (lbs)	Failure Strain (in/in)	Flexural Strength (psi)	Flexural Modulus (10^6 psi)	DR (1580)	
Composite #1						
Untreated	325	0.022	143000	6.83	1.3	
100°C	295	0.021	139000	6.72		
250°C	281	0.020	133000	6.72	1.0	
300°C	25	0.009	11800	3.25		
310°C	39	0.005	19200	4.00		
320°C	38	0.019	16300	2.43		
340°C	10	0.022	3130	0.59	0.8	
100 hr, solar simulator	319	0.021	136000	6.52	1.3	
100 hr solar simulator 40% O_2, 60% H_2	289	0.021	129000	6.34		
100 hr, 100°C, H_2O	316	0.022	135000	6.29	1.5	
					DR (1050)	Raman (1610)
Composite #2						
Untreated	90.5	0.033	45600	2.89	300	11.6
100°C	97.8	0.034	46400	2.88	170	5.9
125°C	94.1	0.051	46700	2.79	270	12.1
150°C	93.9	0.045	45300	2.67	340	18.5
175°C	97.8	0.050	46800	2.53	120	13.8
200°C	99.2	0.044	49600	2.97	280	17.2
225°C	99.6	0.037	45100	2.48	180	9.3
250°C	97.2	0.039	43400	2.43	170	20
275°C	93.0	0.045	46600	2.73	360	23
300°C	102.0	0.036	48600	2.64	140	41
320°C	94.7	0.037	47000	2.70	210	12.0
340°C	99.9	0.043	43400	2.34	270	19
360°C	94.6	0.028	44100	2.80	120	29
380°C	84.9	0.038	42800	2.95	230	34
400°C	87.1	0.032	39800	2.48	150	35
30 hr solar simulator	94.7	0.045	46200	2.72		
100 hr solar simulator	97.5	0.036	49600	3030		
3 hr, 100°C , H_2O	98.7	0.042	48700	2.82		
10 hr, 100°C, H_2O	98.9	0.043	46400	2.96		
30 hr solar simulator 40% O_2, 60% N_2	100.0	0.039	51500	3.03		
100 hr solar simulator 40% O_2, 60% N_2	98.0	0.045	46700	2.75		
					DR (1560)	DR (1735)
Composite #3						
Untreated	247	0.007	101000	14.1	60	340
250°C	605	0.011	160000	15.5	51	260
450°C	460	0.012	128000	13.6		
100 hr, solar simulator	491	0.010	158000	16.5	37	80

4. DISCUSSION

4.a. Correlations

It can be seen in Table 4, that the DR band intensities and mechanical test values show identical trends for composite #1 (although the DR data is less dramatic). Heat clearly weakens this composite, whereas water and ultraviolet radiation have little or no effect. The mechanical test data for composite #3 is not as clearly defined, but again, heat weakens the composite, whereas water and ultraviolet radiation have little effect. The dramatic loss in the DR 1735 cm^{-1} band intensity due to ultraviolet radiation is not supported by the mechanical test data, and requires further investigation.

The mechanical test data was less pronounced for composite #2. This is presumably, because this composite is more pliable and mechanical failure is less pronounced. Nevertheless, again heat resulted in weakening the sample, and water and ultraviolet had little effect. Correlations between the mechanical test data and spectra data are evident in Table 4, but more easily observed by plotting relative values (Figure 47).
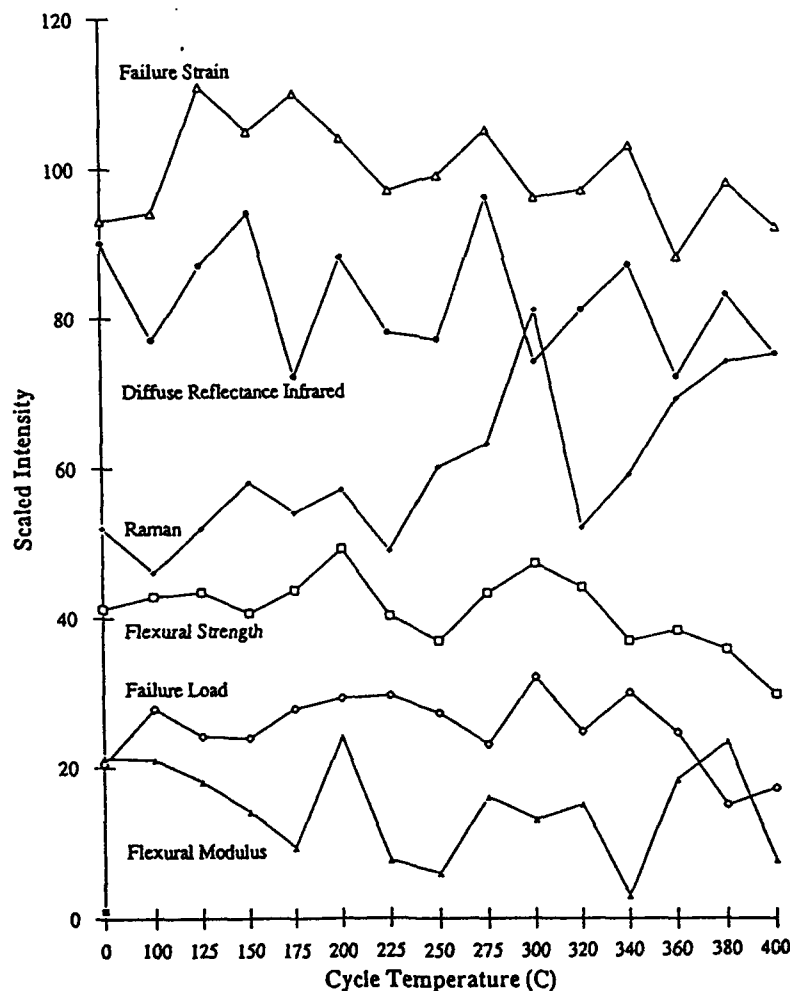

Figure 47. Correlations Between Heat Induced Vibrational Mode and Mechanical Property Changes.

44

The DR infrared band intensity (1050 cm^{-1}), although erratic, correlates rather well to the failure strain, especially at temperatures above 250 °C. The FT-Raman band intensity (1610 cm^{-1}), a little less erratic, can be correlated to flexural strength and failure load up to about 340 °C, at which point the data diverge.

The overall data suggest, that heating this composite degrades the epoxy matrix, which begins to decompose above 300 °C resulting in a loss of mechanical strength. The heating process, however has little or no effect on the Kevlar fibers throughout this range.

4.b. Task 6 - Predictive Abilities.

Initially, a data base was to be established to allow statistical analysis. However, the data sets in Table 4 are insufficient to meet this objective. Nevertheless, the data may be evaluated qualitatively. As previously stated, the measurements are consistent with each other, but were not as expected. In particular, both DR and Raman spectra revealed an increase in band intensities for composite #2 as it was heated. Although, it was initially assumed that bands would decrease with temperature, these results forced us to re-examine the sample degradation process. Identification of the bands as due to Kevlar, not epoxy allowed us to conclude that the latter layer was being removed, revealing the underlying Kevlar. Nevertheless, it is realized that a more extensive data set (higher temperatures for Kevlar/epoxy, and longer or more intense moisture and ultraviolet radiation for all composites) is required to develop equations for the relationships between the measurements and temperature and establish error limits and accurate predictive abilities.

5. CONCLUSIONS

Correlations between FT-Raman and reflectance infrared spectral features to mechanical property tests for thermally degraded Kevlar/epoxy composites were established. The Raman and infrared Kevlar vibration intensities trend changes in flexural strength and failure strain, respectively for thermally degraded composites. These data, along with infrared spectra of evolved species, suggest thermal degradation of Kevlar/epoxy composites occurs in three stages; degradation and removal of the epoxy surface layer (Kevlar band intensities increase), followed by decomposition of the inner matrix (decrease in mechanic strength above 300 °C), and degradation of Kevlar at higher temperatures (gas phase infrared spectrum of p-hydroxy phenyl 2-butone at 450 °C).

REFERENCES

1.   "Cross-linked Polymers: Chemistry, Properties, and Applications" Ed. R. A. Dickie, S. S. Labana, and R. S. Bauer, ACS Symposium Series 367, (1988)

2.   For example; Fiberite (Tempe, AZ), or Narmco (Div. of BASF, Freeport, TX)

3.   Morrison, R.T. and Boyd, R.N., Organic Chemistry, Third Edition, Allyn and Bacon. Inc., Boston, MA, Chapter 32, (1974).

4.   Lee, H. and Neville, K., Handbook of Epoxy Resins, McGraw Hill Book Company, New York, NY, (1982).

5.   Sinclair, R.A., in Ultrastucture Processing of Ceramics, Glasses, and Composites", (Hench, L.L. and Ulrich, D.R., Eds.), John Wiley & Sons, New York, NY, pp 256-264, (1984).

6.   Allcock, H.R. and Lampe, F.W., Contemporary Polymer Chemistry, Prentice Hall, Inc., Englewood Cliffs, NJ, Chapter 21, (1981).

7.   Hunston, D.L., Moulton, R. J., Johnston, N. J. , and Bascom, W. D., ASTM Spec. Tech. Publ., 937, 74-94, (1987).

8.   Hagnauer, G.L., Kleinmeye, J.D., Wixted, J.J., and Grubbs, J. H. "Applications of Digital Image Processing in Testing and Evaluation of Composite Materials", DTIC Report No. AD-A222 939, (1990)

9.   Gardiner, D.S. and Pearson, L.H., J. Acoust. Emiss., 4 (2-3), S199-S202, (1985).

10.   Chen, F., Hiltner, A., and Bear, E., J. Composite Matewrials, 26, 2289-2306 (1992)

11.   H. T. Hahn, "Damage Assessment in Composites by Acousto-Ultrasonic Technique", DTIC Report No. AD-A174 054, (1986)

12.   Haavig, D.L. and King, D.C., Proc. SPIE-Int. Soc. Opt. Eng., 934, 102-110, (1988).

13.   P. V. McLaughlin, Jr. and M. G. Mirchandani, "Aerostructure Nondetructive Evaluation by Thermal Field Detection", Report No. NAEC-92-181 (1984).

14.   Reynolds, G.O., Mueller, P.R., Servaes, D.A., and DeVelis, J.B., Proc. SPIE-Int. Soc. Opt. Eng., 615, 112-117, (1986).

15.   Scotese, A. E., "A low cost shadow Moire device for NDE of impact damage in composite laminates", DTIC Report No. AD-A223 451, (1988)
      Kulkarni, S.V., McLaughlin, P.V., Jr., Pipes, R.B., and Rosen, B.W., ASTM Spec. Tech. Publ., 627, 70-92, (1977).

16.   Coleman, M.M., Xu, Y., and Painter, P.C., Polym. Mater. Sci. Eng., 64, 28-29 (1991),

17.   M. A. Druy, et. al., "In-Situ Composite Cure Monitoring Using Infrared Transmitting Optical Fibers", SAMPE J.,25(2), 11-16 (1989)

18.   Ibid., "FTIR Fiber Optic Monitoring of Composites During Cure in an Autoclave", S.P.I.E.,1170, 150-159 (1989)

19.   Franconi, B.M., J. Test. Eval., 12, (1), 33-39, (1984).

20.   K. C. Cole, D. Noel, and J.-J. Hechler, Applications of Diffuse Reflectance FTIR to Fiber Reinforced Composites", Polymer Composites, 9(6), 395-403 (1988)

21.   M. M. Coleman, D. J. Skrovanek, J. Hu, and P. C. Painter, Macromolecules, 21, 59-65 (1988)- Polyimide cure kinetics with FTIR

22.   Churo, R. and Nishioka, A., Polym. J., 3, 670 (1972)

23.   Matzkanin, G.A., "Investigation of the Effect of Moisture on the Mechanical Properties of Organic Matrix Composite Materials Using Nuclear Magnetic Resonance", Technical Report No. SWRI-15-5607-807, Southwest Research Institute, San Antonio, TX, (1981).

24.   Wang, F.W., Lowry, R.E., and Fanconi, B.M., Polymer, 27, (1), 1529-32, (1986).

25.   Davis, C., "Nondestructive Testing Technology - Army Aircraft", DTIC No. DAOE3834, (1990).

26.   Jones, P.L., "Positron Annihilation Spectroscopy: A Nondestructive, Submicron
       Characterization Technique for Structural Polymers, DTIC No. DA310191, (1990).
27.   Hiemenz, P.C., Polymer Chemistry: The Basic Concepts, Marcel Dekker, Inc., New York,
       NY, Chapter 3, (1984).
28.   Preister, R.D., McClusky, J.V., Cortelek, D.I., Carleton, P.S., Porter, J. R., and
       deHaseth, J. A., Chemical, Biological,, and Environmental Applications of Fibers, (R. A.
       Leiberman, Ed.), Proc. SPIE, (1992) accepted.
29.   Placzek, G., UCRL Translation No. 526L from Handbuch der Radiologie, 2, (E. Marx, Ed.),
       Akademische Verlags Gesellschaft, Leipsag, (1934).
30.   Tobias, R.S., J. Chem. Ed., 44, 2-8, (1967).
31.   Albrecht, A.C. and Hutley, M.C., J. Chem. Phys., 55, 4438-4443, (1971).
32.   Garrison, A.A., Muly, E.C., Roberts, M.J., Trimble, D.S., and Moore, C.F., ISA, Research
       Triangle Park, 357-363, (1989).
33.   Garrison, A.A., "Optically Based Methods for Process Analysis", (D.S. Bomse, H.Brittain, S.,
       Farquharson, J.M. Lerner, A.J. Rein, C. Sohl, T.R., Todd, and L. Weyer, Eds.,), Proc. SPIE,
       1681, (1992) accepted.
34.   McCreery, R.L., Fleischmann, M., and Hendra, P., Anal. Chem. ,55, 146-148, (1983).
35.   McLachlin, R.D., Jewett, G.L., and Evans, J.C., US Patent No. 4,573,761, (1986).
36.   A paper presented by S. Farquharson for Leugers, M.A. and McLachlan, R.D., Chemical,
       Biological, and Environemtnal Applications of Fiber, (R.A. Leiberman and M.T. Wlodarczyk,
       Eds.) Proc. SPIE 990, 88-95, (1988).
37.   Williamson, J.M., Bowling, R.J., and McCreery, R.L., Appl. Spectrosc., 43, 372-375, (1989).
38.   Allred, C.D. and McCreery, R.L., Appl. Spectrosc., 44, 1229-1231, (1990).
39.   Angel, S.M., Vess, T.M., and Myrick, M.L., Chemical, Biological, and Envrionmental Fiber
       Sensors III, (R.A. Lieberman and M.T. Wlodarczyk, Eds.), Proc. SPIE, 1587, 219-231, (1991).
40.   Carrabba, M.M. Spenser, K.M., and Rauh, R.D., in Environmental Sensing and Combustion
       Diagnostics, (J.J. Santoleri, Ed.), Proc. SPIE, 1434, 127-134, (1991).
41.   Farquharson, S., "Optically Based Methods for Process Analysis", (D.S. Bomse, H.Brittain, S.,
       Farquharson, J.M. Lerner, A.J. Rein, C. Sohl, T.R., Todd, and L. Weyer, Eds.,), Proc. SPIE,
       1681, (1992) accepted.
42.   Griffiths, P.R. and deHaseth, J.A. "Fourier Transfrom Infrared Spectroscopy", J.Wiley & Sons,
       Eds. p. 177, 1986).
43.   Tactix and XU-71787 are Trademarks of Dow USA, the structures wer taken from product
       literature.
44.   Four Point Bending experiments and data anlasis were performed by R. Elleithy, T. Ebeling,
       and J. Wallace at Case Western Reserve University, Cleveland, OH.